



# Blow-up dynamics in the mass super-critical NLS equations

Kai Yang<sup>a</sup>, Svetlana Roudenko<sup>a,\*</sup>, Yanxiang Zhao<sup>b</sup>

<sup>a</sup> Department of Mathematics & Statistics, Florida International University, Miami, FL, USA

<sup>b</sup> Department of Mathematics, George Washington University, Washington, DC, USA

## HIGHLIGHTS

- Description of stable blow-up in supercritical nonlinear Schrödinger equation.
- Stable blow-up solutions in supercritical regime have square root blow-up rate.
- Profile equation has multi-bump structure of profile solutions but only one profile describes stable blow-up.
- No significant difference in stable blow-up in energy-critical, sub-or super-critical regimes.

## ARTICLE INFO

### Article history:

Received 2 November 2018

Received in revised form 25 February 2019

Accepted 27 February 2019

Available online 15 March 2019

Communicated by D. Pelinovsky

### Keywords:

NLS equation

Blow-up dynamics

Super-critical collapse

Dynamic rescaling method

Multi-bump profiles

## ABSTRACT

We study stable blow-up dynamics in the  $L^2$ -supercritical nonlinear Schrödinger equation with radial symmetry in various dimensions. We first investigate the profile equation and extend the result of Wang (1990) and Budd et al. (1999) on the existence and local uniqueness of solutions of the cubic profile equation to other  $L^2$ -supercritical nonlinearities and dimensions  $d \geq 2$ . We then numerically observe the multi-bump structure of such solutions, and in particular, exhibit the  $Q_{1,0}$  solution, a candidate for the stable blow-up profile. Next, using the dynamic rescaling method, we investigate stable blow-up solutions in the  $L^2$ -supercritical NLS and confirm the square root rate of the blow-up as well as the convergence of blow-up profiles to the  $Q_{1,0}$  profile.

© 2019 Elsevier B.V. All rights reserved.

## 1. Introduction

Consider the Cauchy problem of the nonlinear Schrödinger (NLS) equation

$$\begin{cases} iu_t + \Delta u + |u|^{p-1}u = 0, & (t, x) \in [0, T) \times \mathbb{R}^d \\ u(x, 0) = u_0 \in H^s(\mathbb{R}^d), s \geq 1. \end{cases} \quad (1.1)$$

During their lifespan, the solutions  $u(x, t)$  of the Cauchy problem (1.1) conserve mass and energy (or Hamiltonian):

$$M[u(t)] \stackrel{\text{def}}{=} \int |u(x, t)|^2 dx = M[u_0], \quad (1.2)$$

$$E[u(t)] \stackrel{\text{def}}{=} \frac{1}{2} \int |\nabla u(x, t)|^2 dx - \frac{1}{p+1} \int |u(x, t)|^{p+1} dx = E[u_0]. \quad (1.3)$$

(The momentum is also conserved, however, we omit it due to the radial setting.)

We are interested in the  $L^2$ -supercritical case of Eq. (1.1), for that we recall the scaling index and scaling invariance. If  $u(x, t)$  solves (1.1), then so does  $\tilde{u}(x, t) = \lambda^{\frac{2}{p-1}} u(\lambda x, \lambda^2 t)$ . A direct calculation shows that the following  $\dot{H}^{s_c}$  norm is invariant under the above scaling, i.e.,  $\|u\|_{\dot{H}^{s_c}} = \|\tilde{u}\|_{\dot{H}^{s_c}}$ , with the critical index defined by

$$s_c = \frac{d}{2} - \frac{2}{p-1}. \quad (1.4)$$

Eq. (1.1) is classified as

- $L^2$ -subcritical (or mass-subcritical) if  $s_c < 0$ ;
- $L^2$ -critical (or mass-critical) if  $s_c = 0$ ;
- intercritical (or mass-supercritical and energy-subcritical) if  $0 < s_c < 1$ ;
- $\dot{H}^1$ -critical (or energy-critical) if  $s_c = 1$ ;
- $\dot{H}^1$ -supercritical (or energy-supercritical) if  $s_c > 1$ .

The well-posedness of solutions to Eq. (1.1) has been long investigated starting with works by Ginibre and Velo in [1], see also [2] and references therein. We discuss separately cases  $s_c \leq 1$  and  $s_c > 1$ . When  $s_c \leq 1$ , the local well-posedness is available in  $H^1(\mathbb{R}^d)$ , implying that for  $u_0 \in H^1(\mathbb{R}^d)$  there exists  $0 < T \leq \infty$

\* Corresponding author.

E-mail addresses: [yangk@fiu.edu](mailto:yangk@fiu.edu) (K. Yang), [sroudenko@fiu.edu](mailto:sroudenko@fiu.edu) (S. Roudenko), [yxzhao@gwu.edu](mailto:yxzhao@gwu.edu) (Y. Zhao).

such that there is a unique solution  $u(t) \in \mathbb{C}([0, T), H^1(\mathbb{R}^d))$ . We say the solution exists globally in time if  $T = \infty$ , and the solution blows up in finite time if  $T < \infty$  and  $\limsup_{t \nearrow T} \|\nabla u(t)\|_{L^2} = \infty$ . When  $s_c > 1$ , taking the Schwartz class initial data  $u_0 \in \mathcal{S}(\mathbb{R}^d)$ , local well-posedness is obtained in  $H^s$  with  $s > s_c$ . As discussed in [3], solutions of Eq. (1.1) may  $H^s$ -blow up at time  $T^*$ , that is  $\lim_{t \rightarrow T^*} \|u(t)\|_{\dot{H}^s} = \infty$ , and persistence of regularity yields that  $T^*$  is unique with respect to the norms  $H^{\tilde{s}}$ ,  $\tilde{s} > s_c$ . Hence, while the local  $H^1$  theory is absent in this case, there is still a clear distinction between global solutions ( $T = \infty$ ) and finite-time blow-up solutions ( $T < \infty$ ) for  $s_c > 1$ .

Solutions to Eq. (1.1) when  $s_c \geq 0$  may blow-up in finite time. A typical argument to show the existence of such blow-up solutions is the convexity argument for the negative energy initial data ( $E[u_0] < 0$ ) with finite variance ( $V[u_0] \stackrel{\text{def}}{=} \int |xu_0|^2 < \infty$ ). When  $s_c < 0$ , solutions to (1.1) exist globally in time, for example, see [4]. The first attempt to study stable blow-up solutions was in the mass-critical case ( $s_c = 0$ ), where there has been good progress in both analytical and numerical descriptions, see [5–12], and references therein. In this case, the dynamics of finite-time stable blow-up is described as follows: solutions have the “log-log” blow-up rate

$$\|\nabla u(t)\|_2 \sim \left( \frac{\ln \ln \left( \frac{1}{T-t} \right)}{T-t} \right)^{\frac{1}{2}} \quad \text{as } t \rightarrow T,$$

for example, see [12–21]; and the blow-up profiles are given by the (unique positive) ground state solution of the nonlinear elliptic equation

$$-Q + \Delta Q + |Q|^{p-1}Q = 0, \quad Q \in H^1(\mathbb{R}^d). \quad (1.5)$$

In this paper, we investigate stable blow-up solutions in the mass-supercritical case  $s_c > 0$ . To be specific, we consider radial solutions  $u(r, t)$  to Eq. (1.1),  $r = |x|$ ,  $x \in \mathbb{R}^d$ . For consistency with previous work (e.g., [5,13,14]), we set  $\sigma = \frac{p-1}{2}$  and write the nonlinear term as  $|u|^{2\sigma}u$ ; note that in this notation  $s_c = \frac{d}{2} - \frac{1}{\sigma}$ . Due to the scaling invariance we can rescale solutions to the NLS equation in the radial setting with a scaling function  $L(t)$  (e.g.,  $L(t) = 1/\|u(t)\|_\infty^\sigma$ , for other options see [14,22])

$$u(r, t) = \frac{1}{L(t)^{\frac{1}{\sigma}}} v(\xi, \tau), \quad \text{where } \xi = \frac{r}{L(t)}, \quad \tau = \int_0^t \frac{ds}{L(s)^2}. \quad (1.6)$$

Then Eq. (1.1) becomes

$$iv_\tau + ia(\tau) \left( \xi v_\xi + \frac{v}{\sigma} \right) + \Delta v + |v|^{2\sigma}v = 0, \quad (1.7)$$

where

$$a(\tau) = -L \frac{dL}{d\tau} = -\frac{d \ln L}{d\tau}. \quad (1.8)$$

The second term in (1.7), containing  $a(\tau)$ , makes a fundamental difference in the blowup behavior between the mass-critical and supercritical cases, this is due to the limiting behavior of  $a(\tau)$ . As discussed, for example, in [5] or [23], the stable blow-up dynamics will correspond to  $a(\tau) \rightarrow a$ , a constant, as the rescaled time  $\tau \rightarrow \infty$ . If  $a(\tau)$  converges to zero,<sup>1</sup> then stable singular solutions to Eq. (1.1) blow-up at the square root rate with the “log-log” correction (and that happens exactly in the  $L^2$ -critical case, see, [5,11,12,14,22,24]). If  $a(\tau)$  converges to a non-zero constant, then solutions to (1.1) blow up at the square root rate without any correction in the leading term. This characterizes

the  $L^2$ -supercritical stable blow-up, see [5,11,14]. Therefore, understanding the behavior of  $a(\tau)$  sheds light onto the rate of the stable blow-up solutions in Eq. (1.1).

A more challenging task is to understand and describe the blow-up profiles. Following the setting of Zakharov [23] (see also details in [25])  $v(\xi, \tau) = e^{i\tau}Q(\xi)$  and considering  $a(\tau) \rightarrow a$  as  $\tau \rightarrow \infty$ , we obtain

$$\Delta_\xi Q - Q + ia \left( \frac{Q}{\sigma} + \xi Q_\xi \right) + |Q|^{2\sigma}Q = 0. \quad (1.9)$$

We refer to this equation as the *profile equation*. The desired solutions of (1.9) satisfy

$$Q_\xi(0) = 0, \quad Q(0) = \text{real}, \quad \text{and} \quad Q(\infty) = 0. \quad (1.10)$$

Accordingly, we investigate the profile equation (1.9) with conditions (1.10).

Note that in the critical setting ( $s_c = 0$ ), the value  $a = 0$ , and thus, Eq. (1.9) is reduced to (1.5), the ground state equation.

As predicted by Zakharov in [23] (see also [24]), stable blow-up solutions are expected to be of the self-similar form

$$u(x, t) = \frac{1}{L(t)^{\frac{1}{\sigma}}} Q \left( \frac{x}{L(t)} \right) \exp \left( i\theta + \frac{i}{2a} \log \frac{T}{T-t} \right), \quad (1.11)$$

where

$$L(t) = (2a(T-t))^{1/2}. \quad (1.12)$$

The existence theory for such solutions  $Q$  was first shown by X.-P. Wang in his thesis [26] for the 3d cubic case, he also showed that in the cubic case  $Q(x)$  decays as  $1/|x|$  when  $|x| \rightarrow \infty$ . Later in [27], Budd, Chen and Russell, using the Volterra integral equation theory, extended the existence results for the cubic NLS cases in the inter-critical regime, i.e., when  $0 < s_c < 1$  or  $2 < d < 4$ . They also showed the  $1/|x|$  decay of such solutions  $Q$  in the cubic case.

The first numerical evidence of monotone decreasing solutions to the profile equation (1.9) for the 3d cubic and 2d quintic NLS cases was given in [28]. There it was also shown that the asymptotic behavior of solutions to (1.9)–(1.10) (for any  $\sigma > 0$ ), in the form of (1.11), includes for  $Q(\xi)$  two linearly independent solutions for large  $\xi$ :

$$Q_1 \approx |\xi|^{-\frac{i}{a}-\frac{1}{\sigma}} \quad \text{and} \quad Q_2 \approx e^{-\frac{ia\xi^2}{2}} |\xi|^{\frac{i}{a}-d+\frac{1}{\sigma}},$$

and thus,  $Q$  can be written as  $Q = \alpha Q_1 + \beta Q_2$  when  $\xi \rightarrow \infty$  (with  $\alpha, \beta \in \mathbb{C}$ ). Substituting the ansatz (1.11) into the formulas for conserved quantities, we obtain the following expressions for the mass and energy (here,  $\omega_d$  - the surface area of the  $d-1$ -dimensional unit sphere):

$$M[u(t)] = L(t)^{2s_c} \omega_d \int_0^\infty |Q(\xi)|^2 \xi^{d-1} d\xi, \quad (1.13)$$

$$E[u(t)] = L(t)^{2(s_c-1)} \frac{\omega_d}{2} \times \int_0^\infty \left[ |\nabla Q(\xi)|^2 - \frac{1}{\sigma+1} |Q(\xi)|^{2(\sigma+1)} \right] \xi^{d-1} d\xi. \quad (1.14)$$

For the profile solutions  $Q$  and to simplify the notation (getting rid of  $\omega_d$  and the factor  $\frac{1}{2}$  in (1.14)), we denote the Hamiltonian of  $Q$  as  $H[Q]$ , or the integral in (1.14)

$$H[Q] \stackrel{\text{def}}{=} \int_0^\infty \left[ |\nabla Q(\xi)|^2 - \frac{1}{\sigma+1} |Q(\xi)|^{2(\sigma+1)} \right] \xi^{d-1} d\xi.$$

When  $0 < s_c < 1$ , the energy of the self-similar blow-up in (1.14) must be finite, and hence, the Hamiltonian of  $Q$  must be zero:  $H[Q] = 0$  (since  $L(t) \rightarrow 0$  as  $t \rightarrow T$ ). Similarly, the mass of  $u$  in (1.13) remains constant, and thus, the  $L^2$  norm of  $Q$  is unbounded.

<sup>1</sup> For example, in [5,12,14] the convergence of  $a(\tau)$  is at the rate  $1/(\ln \tau + 3 \ln \ln \tau)$ .

In summary,  $Q = \alpha Q_1 + \beta Q_2$  is in  $\dot{H}^1$  but not in  $L^2$ . Though both  $Q_1$  and  $Q_2$  vanish at infinity, the fast oscillating span  $Q_2$  should be excluded from consideration (or one has to choose only those parameters  $Q(0)$  and  $a$ , which generate the solutions to (1.9) with  $\beta \equiv 0$ ). Thus, the next natural step is to understand the  $Q_1$ -type solutions, or solution to (1.9) with boundary conditions

$$Q_\xi(0) = 0, \quad Q(0) = \text{real}, \quad Q(\infty) = 0, \quad H[Q] = 0. \quad (1.15)$$

As far as the uniqueness, the *local* uniqueness was shown in [27]: for any given  $Q(0) \in \mathbb{R}$  and constant  $a > 0$ , Eqs. (1.9)–(1.15) has a unique solution. The obvious question then is, which  $Q(0)$  and  $a$  produce solutions that would match the profiles of the stable blow-up solutions of (1.1) from generic initial data.

It should be mentioned that prior to [27], Kopell and Landman in [29] constructed such a unique profile  $Q$  in the cubic case when the dimension  $d$  is exponentially asymptotically close to 2. (Using this result, Merle, Raphaël, and Szeftel in [30] constructed stable blow-up solutions in the cubic case when  $d \gtrsim 2$ .) In [31] Rottshäfer and Kaper improved the construction to include settings where the dimension  $d$  is algebraically close to 2, i.e.,  $d(a) = 2 + O(a^l)$  for  $l > 0$ . The physical case of the 3d cubic NLS, however, is in no way close to the dimension 2, consequently, the above perturbative approaches (the only ones currently available for  $Q$  construction) leave the question of profile(s)  $Q$  open.

LeMesurier, Papanicolaou, Sulem and Sulem in [28], while considering several generic initial conditions and solving the equation numerically via the dynamic rescaling method that they introduced, found that  $a(\tau)$  tends to some specific constant, for example, in the 3d cubic NLS  $a = 0.917\dots$ ;  $Q(0)$  has also a specific value,  $Q(0) = 1.885\dots$ . They observed that the values of  $a$  and  $Q(0)$  are very sensitive to perturbations, even 4% deviation would generate a nontrivial perturbation and would not generate a profile with non-oscillating tail. Despite such a sensitivity, it is remarkable that the authors in [28] were able to identify the above parameters with such precision; furthermore, they investigated the case of the 2d quintic NLS and obtained  $a = 1.533\dots$  and  $Q(0) = 1.287\dots$  in that setting.

Budd, Chen and Russell in [27] numerically studied the cubic NLS in  $2 < d < 4$ , and found that the span of  $Q_1$  solutions to Eqs. (1.9)–(1.15) is large: an infinite (at least a countable) number of distinct self-similar solutions (with monotone decay at infinity, or in other words, with non-oscillatory tails), which are characterized by the number of maxima of  $|Q|$  when the dimension  $d$  is close to 2, and thus, called ‘multi-bump’ solutions. Among those solutions, only one monotonically decreasing solution, denoted by  $Q_{1,0}$ , is the actual profile of the *stable* blow-up (from the generic initial data) in the cubic NLS equation. It is indeed the only monotone solution when the dimension is asymptotically close to 2. As the dimension increases away from two, there may be other monotone solutions as was demonstrated for the cubic NLS in [27], we also show examples of several monotone solutions for other nonlinearities in Section 3, see Figs. 3–4. Observe that the profile  $Q_{1,0}$  is exactly the one found by LeMesurier, Papanicolaou, Sulem and Sulem in [28]. We provide some more details about the profile solutions  $Q_{j,K}$  in Section 3 and show examples; for further reading on the structure of profile solutions as well as estimates on the location and value of the maxima, see [27,32]; for further discussion on numerical treatments refer to [5,15,33,34]. An attempt to investigate multi-bump solutions analytically, via dynamical systems approach, was done by Rottshäfer and Kaper in a very interesting paper [35]. There, far range asymptotics was glued to the origin, resulting in the so-called midrange part, where non-monotone behavior is possible, and that led to a variety of multi-bump solutions.

We also note that the papers [29,31,35] are the only analytical constructions of  $Q$  in the mass-supercritical setting.

In this paper, we investigate mass-supercritical cases of the NLS equation, including energy-supercritical cases. We first show the existence and local uniqueness of solutions to the profile equations (1.9)–(1.10), including nonlinearities  $p \neq 3$ , and review the decay of  $Q$  solutions. We then investigate the profile equation (1.9) and study the multi-bump solutions  $Q_{j,K}$  numerically for the specific powers of nonlinearities  $p = 3, 5, 7$  (or  $\sigma = 1, 2, 3$ ) in a variety of dimensions (from two to five). Finally, using the dynamic rescaling method, we obtain stable blow-up solutions to the NLS equations and show that the rate of the blow-up is indeed given by (1.12) and the blow-up profiles converge to the specific solution  $Q_{1,0}$  of the profile equation (1.9) with (1.15).

The paper is organized as follows: in Section 2, we discuss the existence and uniqueness theory for solutions of (1.9)–(1.10) to all mass-supercritical cases for  $d \geq 2$ , as well as the decay of  $Q$  as  $|x| \rightarrow \infty$ . In Section 3, we provide a numerical method to obtain the solutions  $Q$  to (1.9) & (1.10), and in particular, numerically identify the profiles  $Q_{1,0}$ . We observe no difference in obtaining  $Q$  solutions for  $s_c < 1$ ,  $s_c = 1$  and  $s_c > 1$ , though these three cases lead, respectively, to the zero Hamiltonian, constant Hamiltonian and negative Hamiltonian solutions from our numerical observations (the negative Hamiltonian solutions are actually due to the finite interval, we show that the Hamiltonian decreases to negative infinity as the computational domain increases). In Section 4, we simulate the blow-up solutions by the dynamic rescaling method and show the results of convergence of blow-up solutions to the profiles  $Q_{1,0}$  and the square root rate of the blow-up. We provide various error estimates between the blow-up rate and the predicted rate. All the error quantities are satisfactorily small (e.g., on the order  $10^{-5}$ ). Such behaviors are observed among all considered cases with  $0 < s_c < 1$ ,  $s_c = 1$  and  $s_c > 1$ .

## 2. Existence theory of $Q$

### 2.1. Existence of $Q$ for general nonlinearity in radial setting

We start with the existence theory of Eqs. (1.9)–(1.10), which is derived from Eq. (1.7) as a stationary solution by separation of variables  $v(\xi, \tau) = e^{i\tau} Q(\xi)$  (recall  $\xi$  and  $\tau$  from (1.6)). Denoting  $\lim_{\tau \rightarrow \infty} a(\tau) = a$ , we obtain

$$\begin{cases} \Delta_\xi Q - Q + ia \left( \frac{Q}{\sigma} + \xi Q_\xi \right) + |Q|^{2\sigma} Q = 0, \\ Q_\xi(0) = 0, \quad Q(0) = \text{real}, \quad \text{and} \quad Q(\infty) = 0. \end{cases} \quad (2.1)$$

Here,  $\sigma > 0$ , and  $\Delta_\xi := \partial_{\xi\xi} + \frac{d-1}{\xi} \partial_\xi$  denotes the Laplacian with the radial symmetry.

This equation is the key to understanding the profiles for the stable blow-up solutions in the mass-supercritical case. In the cubic case ( $\sigma = 1$ ), the existence of solutions to (2.1) was shown in [5,14,26,27]. Here, we consider mass-supercritical cases with  $d \geq 2$  and  $p > 1$ , or  $\sigma > 0$ . First, we discuss some useful properties of solutions, then we address the question of existence by incorporating the approach from [27], and close this section with an alternative proof of existence using the method from [26], which also gives decay estimates.

**Lemma 2.1.** *If  $Q(\xi)$  is the solution of Eq. (2.1) in any dimension  $d$ , then, it satisfies the identities*

$$\left| \xi Q_\xi + \frac{Q}{\sigma} \right|^2 + 2 \left( d - 2 - \frac{1}{\sigma} \right) \int_0^\xi s |Q_s|^2 + \left( 2 - \frac{2}{\sigma} \right) \int_0^\xi s |Q|^2 \quad (2.2)$$

$$- \frac{d-2}{\sigma} |Q(0)|^2 - \xi^2 |Q|^2 + \left( \frac{d-2}{\sigma} - \frac{1}{\sigma^2} \right) |Q(\xi)|^2 \\ + \frac{1}{\sigma+1} \xi^2 |Q|^{2\sigma+2} + \frac{2}{\sigma(\sigma+1)} \int_0^\xi s |Q|^{2\sigma+2} = 0,$$

and

$$2 \operatorname{Im}(\xi Q_\xi \bar{Q}) + 2(d-2) \operatorname{Im} \int_0^\xi Q_s \bar{Q} + 2a \left( \frac{1}{\sigma} - 1 \right) \\ \times \int_0^\xi s |Q|^2 + a |\xi|^2 |Q|^2 = 0. \quad (2.3)$$

**Proof.** The identity (2.2) is obtained by multiplying the equation in (2.1) by  $2\xi(\xi Q_\xi + \frac{Q}{\sigma})$ , taking the real part and then integrating from 0 to  $\xi$ . The identity (2.3) is obtained by multiplying the equation in (2.1) by  $2\xi \bar{Q}$ , taking the imaginary parts and then integrating from 0 to  $\xi$ .  $\square$

In the next lemma we show the boundedness of solutions to (2.1). Recall  $s_c = \frac{d}{2} - \frac{1}{\sigma}$  and  $\sigma > 0$ .

**Lemma 2.2.** *If  $s_c > 0$ ,  $d > 1 + \frac{1}{\sigma}$ , and  $Q$  is the  $C^2$  solution of (2.1), then  $|Q(\xi)|$  is bounded for all  $\xi > 0$ .*

**Proof.** First note that a  $C^2$  solution to (2.1) is bounded on a finite interval  $\xi \in [0, M]$  for any finite  $M > 0$ . Therefore, it suffices to show boundedness of  $Q$  for  $\xi > M$ , or as  $\xi \rightarrow \infty$ . For that we first rewrite the identity (2.2) as follows

$$\frac{1}{\xi^2} \left| \xi Q_\xi + \frac{Q}{\sigma} \right|^2 + |Q|^2 \left( \frac{1}{\sigma+1} |Q|^{2\sigma} - 1 \right) \\ + \frac{1}{\xi^2} \left( \frac{d-2}{\sigma} - \frac{1}{\sigma^2} \right) |Q|^2 \\ + \frac{1}{\xi^2} \left( 2 - \frac{2}{\sigma} \right) \int_0^\xi s |Q|^2 \\ + \frac{2}{\sigma(\sigma+1)\xi^2} \int_0^\xi s |Q|^{2\sigma+2} \\ = \frac{1}{\xi^2} \left( \frac{d-2}{\sigma} |Q(0)|^2 + 2 \left( 2 + \frac{1}{\sigma} - d \right) \int_0^\xi s |Q_s|^2 \right). \quad (2.4)$$

Our claim is that if  $|Q_\xi|$  is bounded, then so is  $|Q|$ . To the contrary, suppose that  $|Q|$  is not bounded, that is,  $|Q(\xi)| \rightarrow \infty$  as  $\xi \rightarrow \infty$ . By combining the second and third terms in the left-hand side (LHS) of (2.4), we obtain

$$|Q|^2 \left[ \frac{1}{\sigma+1} |Q|^{2\sigma} - 1 + \frac{1}{\xi^2} \left( \frac{d-2}{\sigma} - \frac{1}{\sigma^2} \right) \right].$$

Observe that since  $|Q| \rightarrow \infty$  by our assumption, the first term with  $|Q|^{2\sigma}$  in the square brackets is dominant (and grows as  $\xi$  grows), and the last term is decreasing as  $\xi^{-2}$  regardless of the sign in  $\frac{d-2}{\sigma} - \frac{1}{\sigma^2}$ , and thus, the whole expression is increasing to infinity as  $\xi \rightarrow \infty$ , so for sufficiently large  $\xi$  it will certainly be positive. Adding the second line from (2.4) and comparing it with the entire expression, we obtain for large enough  $\xi$

$$0 \leq |Q|^2 \left[ \frac{1}{\sigma+1} |Q|^{2\sigma} - 1 + \frac{1}{\xi^2} \left( \frac{d-2}{\sigma} - \frac{1}{\sigma^2} \right) \right] \\ + \frac{1}{\xi^2} \int_0^\xi s |Q|^2 \left[ \frac{2}{\sigma(\sigma+1)} |Q|^{2\sigma} + \left( 2 - \frac{2}{\sigma} \right) \right] ds \\ \leq \text{LHS of (2.4)} \\ = \text{RHS of (2.4)}. \quad (2.5)$$

Now, the RHS of (2.4) has two terms: the first term behaves as  $\frac{c}{\xi^2}$  and the integral in the second term is on the order of  $c \xi^2$  as

$\xi \rightarrow \infty$  (recalling the hypothesis  $|Q_\xi|$  being bounded). Hence, overall, the RHS is bounded by a constant when  $\xi \rightarrow \infty$ . This gives a contradiction as the left side in the inequality (2.5) grows to  $\infty$  as  $\xi \rightarrow \infty$ , while the RHS remains bounded. Therefore, we conclude that  $|Q|$  cannot grow to infinity as  $\xi \rightarrow \infty$  and has to be bounded provided  $|Q_\xi|$  is bounded.

Next, we show that  $|Q_\xi|$  is indeed bounded when  $\xi \rightarrow \infty$ . Again, we prove the boundedness of  $|Q_\xi|$  by contradiction. Suppose  $|Q_\xi|$  is not bounded, that is  $\limsup_{\xi \rightarrow \infty} |Q_\xi(\xi)| = \infty$ . Then, there exists a monotonically increasing sequence  $\{\xi_j\}_0^\infty$  for both  $\xi_j$  and  $Q(\xi_j)$  such that  $|Q_\xi(\xi_j)| \rightarrow \infty$  as  $\xi_j \rightarrow \infty$ , and  $|Q_\xi(\xi_j)| > |Q_\xi(\xi_k)|$  for  $j > k$ .

For the RHS of the identity (2.4), we first consider the case when  $2 + \frac{1}{\sigma} - d \leq 0$  (or  $d \geq 2 + \frac{1}{\sigma}$ ). Then the RHS is negative. On the other hand, the LHS of (2.4), is always positive. We consider separately the case when  $Q$  is bounded and when  $Q$  is unbounded. If  $Q$  is bounded, we move the “possible negative terms”  $\frac{1}{\xi^2} (\frac{d-2}{\sigma} - \frac{1}{\sigma^2}) |Q|^2$  and  $|Q|^2 (\frac{1}{\sigma+1} |Q|^{2\sigma} - 1)$  in (2.4) to the RHS and then put the prior bound of  $|Q|$  on the terms  $\frac{1}{\xi^2} (\frac{d-2}{\sigma} - \frac{1}{\sigma^2}) |Q|^2$  and  $|Q|^2 (\frac{1}{\sigma+1} |Q|^{2\sigma} - 1)$ . Then, these two terms will be absorbed by a constant  $c$  and the RHS will still be negative by choosing sufficiently large  $j$ . If  $Q$  is not bounded, then all the terms in the LHS of the identity (2.4) are positive. In both cases, we obtain the identity with strictly positive LHS and strictly negative RHS for some sufficiently large  $\xi_j$ . Therefore, we reach a contradiction in the case  $2 + \frac{1}{\sigma} - d \leq 0$  as  $\xi \rightarrow \infty$ .

Now we consider the case  $2 + \frac{1}{\sigma} - d > 0$  (or  $1 + \frac{1}{\sigma} < d < 2 + \frac{1}{\sigma}$ ). In this case, the RHS of the identity (2.4) satisfies

$$c + \frac{2(2 + \frac{1}{\sigma} - d)}{\xi_j^2} \int_0^{\xi_j} s |Q_s(s)|^2 ds \\ \leq c + \frac{2(2 + \frac{1}{\sigma} - d)}{\xi_j^2} \int_0^{\xi_j} s |Q_s(\xi_j)|^2 ds \\ = c + \left( 2 + \frac{1}{\sigma} - d \right) |Q_\xi(\xi_j)|^2. \quad (2.6)$$

Since  $d > 1 + \frac{1}{\sigma}$ , there exists  $\delta > 0$  such that  $1 - \delta > 2 + \frac{1}{\sigma} - d$  (that is,  $0 < \delta < d - 1 - \frac{1}{\sigma}$ ). Again we discuss two options for  $Q$ :  $Q$  being bounded or  $Q$  being unbounded. If  $Q$  is bounded, we move the “possible negative terms”  $\frac{1}{\xi^2} (\frac{d-2}{\sigma} - \frac{1}{\sigma^2}) |Q|^2$  and  $|Q|^2 (\frac{1}{\sigma+1} |Q|^{2\sigma} - 1)$  in (2.4) to the RHS and then put the prior bound on  $|Q|$ . These two terms will be absorbed by a constant  $c$ . If  $Q$  is not bounded, then all terms in the LHS of the identity (2.4) are not negative. In both scenarios, we obtain

$$(1 - \delta) |Q_\xi(\xi_j)|^2 < \text{LHS of (2.4)} \\ \leq c + (2 + \frac{1}{\sigma} - d) |Q_\xi(\xi_j)|^2. \quad (2.7)$$

Note that  $1 - \delta > 2 + \frac{1}{\sigma} - d$ , and hence, we reach a contradiction in the inequality (2.7) by choosing a sufficiently large  $\xi_j$ . Therefore, we conclude that  $|Q_\xi|$  is bounded. Combining the cases of  $\xi < M$  and  $\xi \rightarrow \infty$ , we conclude that  $|Q(\xi)|$  is bounded for all  $\xi > 0$ .  $\square$

**Remark 2.3.** The only limitation for extending our results to  $d = 1$  is the argument on choosing the parameter  $\delta > 0$ , where we want  $1 - \delta > 2 + \frac{1}{\sigma} - d$  to be true. This implies that we need  $2 + \frac{1}{\sigma} - d < 1$ , implying  $d > 1 + \frac{1}{\sigma} > 1$ .

Before we state our existence and uniqueness results for Eq. (2.1), we recall three lemmas on Volterra integral equations from [36] on existence, continuity and extension of solutions.

**Lemma 2.4** (Existence and Uniqueness for the Volterra Integral Equation). *Consider the Volterra integral equation*

$$x(t) = f(t) + \int_0^t g(t, s, x(s)) ds. \quad (2.8)$$

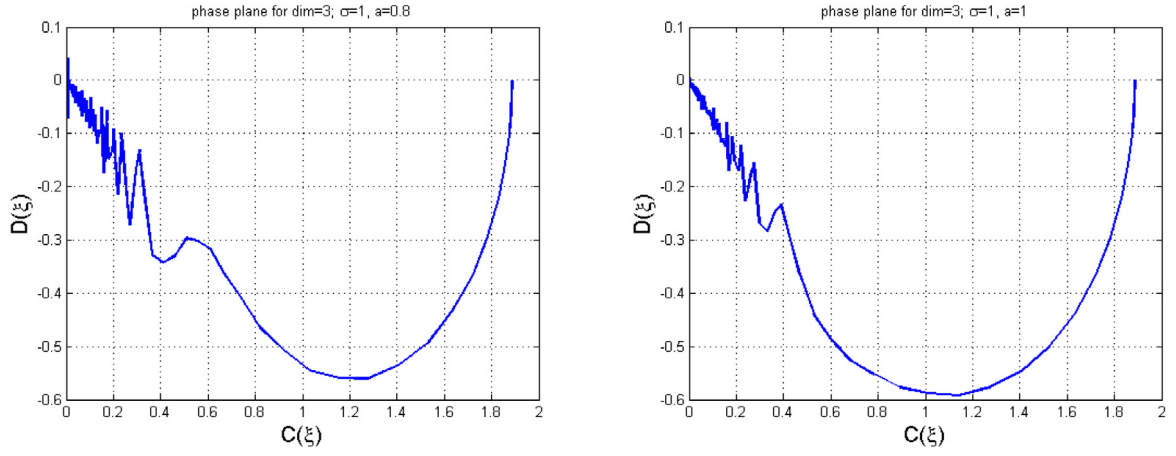


**Fig. 1.**  $Q$  solutions in the coordinates  $(C, D)$  for different values of parameter  $a$  with fixed value of  $Q(0) \equiv Q_{1,0}(0)$ . Left:  $a = 0.8$ . Right:  $a = 1$ . Both solutions show fast oscillating behavior when approaching the origin, thus, not suitable candidates for the blow-up profiles (the value of  $a$  with no oscillations is close to 0.9).

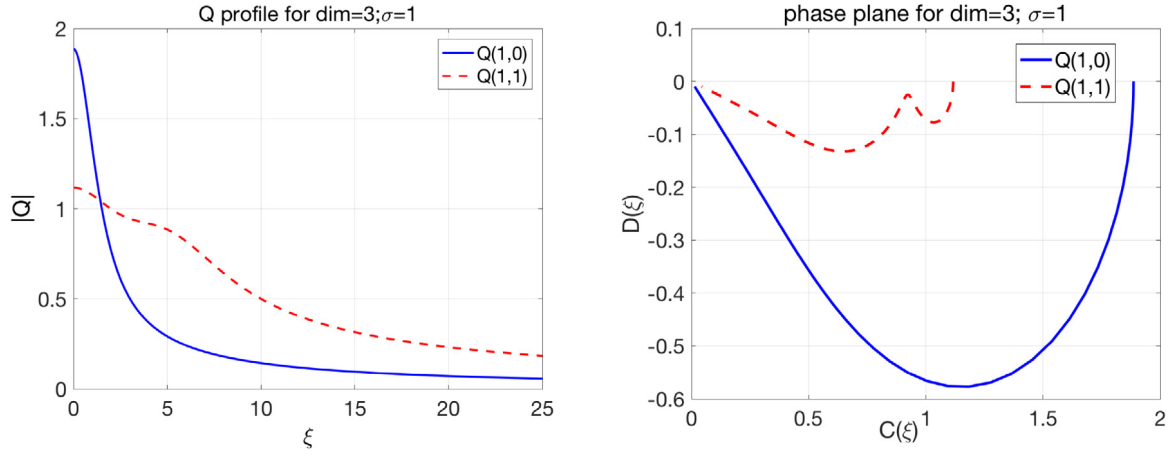


**Fig. 2.**  $Q$  profiles (we plot  $|Q|$ ). Left: The blue curve is the first solution  $Q_{1,0}$  in the branch  $Q_{1,j}$  and the red one is the first bifurcation solution  $Q_{1,1}$ . Right: The phase plane for the 3d cubic case in coordinates  $(C, D)$ .

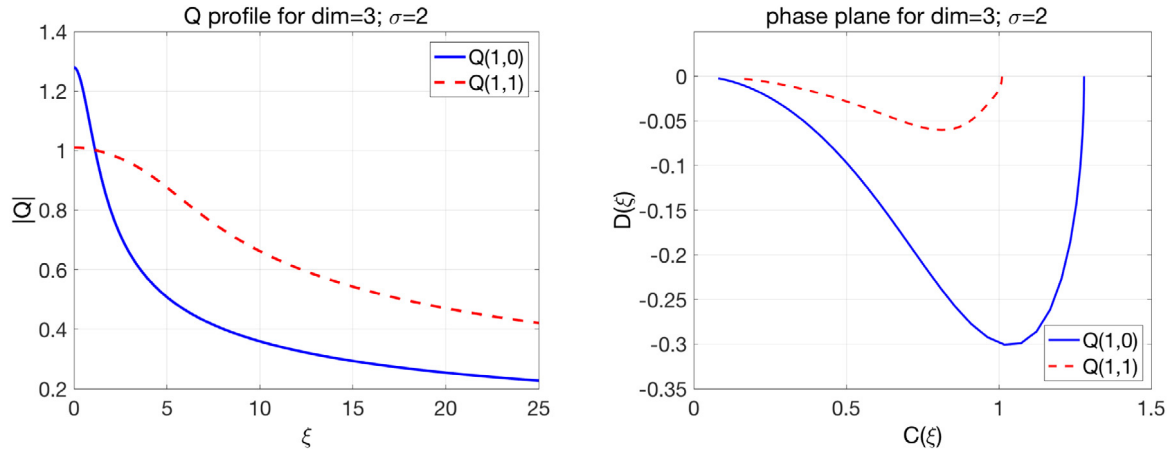


**Fig. 3.**  $Q$  profiles for  $d = 3$ ,  $\sigma = 2$  (left) and the phase plane for  $Q$  (right).

Let  $a, b$  and  $L$  be positive numbers, and for some fixed  $\alpha \in (0, 1)$  we define  $c = \alpha/L$ . Suppose

- $f$  is continuous on  $[0, a]$ ,
- $g$  is continuous on  $U = \{(t, s, x) : 0 \leq s \leq t \leq a \text{ and } |x - f(t)| \leq b\}$ ,

- $g$  is Lipschitz with respect to  $x$  on  $U$ , i.e.,  $|g(t, s, x) - g(t, s, y)| \leq L|x - y|$ , if  $(t, s, x), (t, s, y) \in U$ .

If  $M = \max_U |g(t, s, x)|$ , then there exists a unique solution of (2.8) on  $[0, T]$ , where  $T = \min[a, b/M, c]$ .

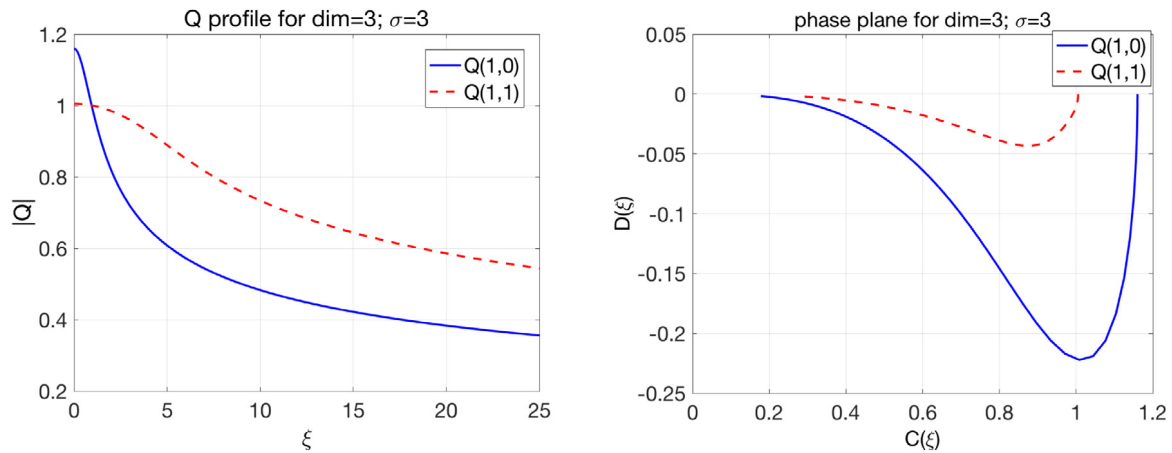


Fig. 4.  $Q$  profiles for  $d = 3$ ,  $\sigma = 3$  (left) and the phase plane for  $Q$  (right).

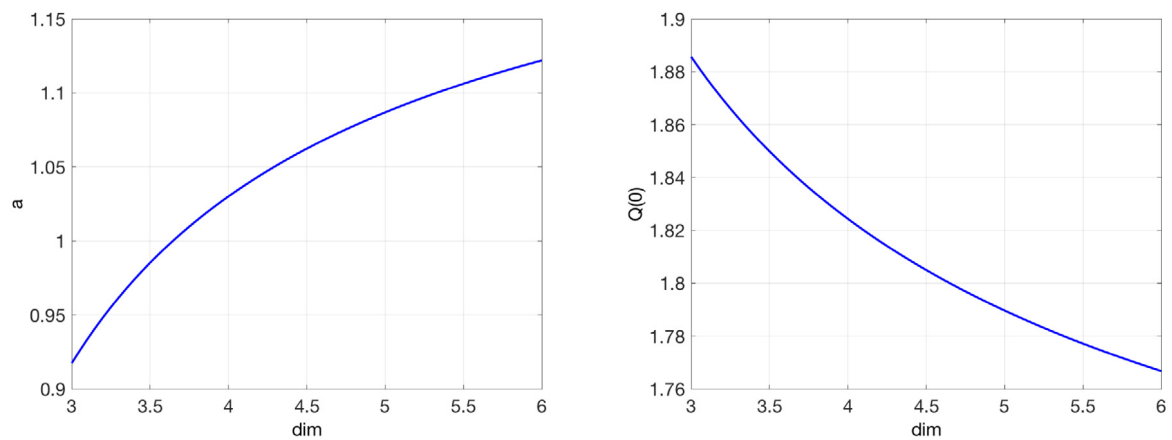


Fig. 5. The change of  $a$  and  $Q(0) = Q_{1,0}(0)$  with respect to the dimension  $d$  for the cubic case ( $\sigma = 1$ ).

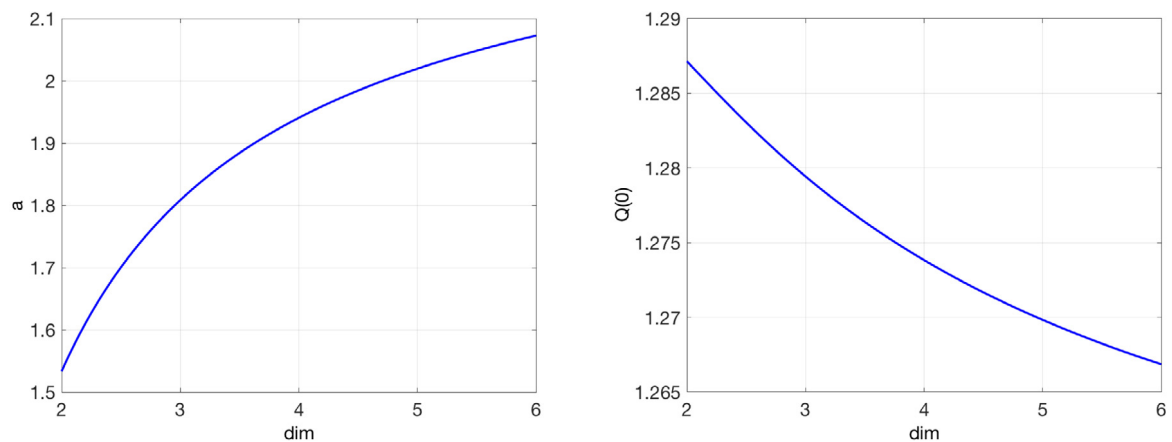


Fig. 6. The change of  $a$  and  $Q(0) = Q_{1,0}(0)$  with respect to the dimension  $d$  for the quintic case ( $\sigma = 2$ ).

**Lemma 2.5** (Continuity for the Volterra Integral Equation). Let  $f : [0, a] \rightarrow \mathbb{R}$  and  $g : U \rightarrow \mathbb{R}$  both be continuous, where  $U = \{(t, s, x) : 0 \leq s \leq t \leq a \text{ and } |x - f(t)| \leq b\}$ . Then there exists a continuous solution of (2.8) on  $[0, T]$ , where  $T = \min[a, b/M]$  and  $M = \max_U |g(t, s, x)|$ .

**Lemma 2.6** (Extension of the Solution). Let  $f : [0, \infty) \rightarrow \mathbb{R}$  and  $g : U \rightarrow \mathbb{R}$  be continuous, where  $U = \{(t, s, x) : 0 \leq s \leq t \leq a \text{ and } |x - f(t)| \leq b\}$ . If  $x(t)$  is a solution of (2.8) on an interval

$[0, T]$ , then there exists a  $\tilde{T} > T$  such that  $x(t)$  can be continued to  $[0, \tilde{T}]$ .

**Theorem 2.1** (Existence and Uniqueness of  $Q$ ). If  $s_c > 0$  and  $d \geq 2$ , for any given initial value  $Q(0) \in \mathbb{R}$  and a constant  $a > 0$ , Eq. (2.1) has a unique  $C^2$  solution.

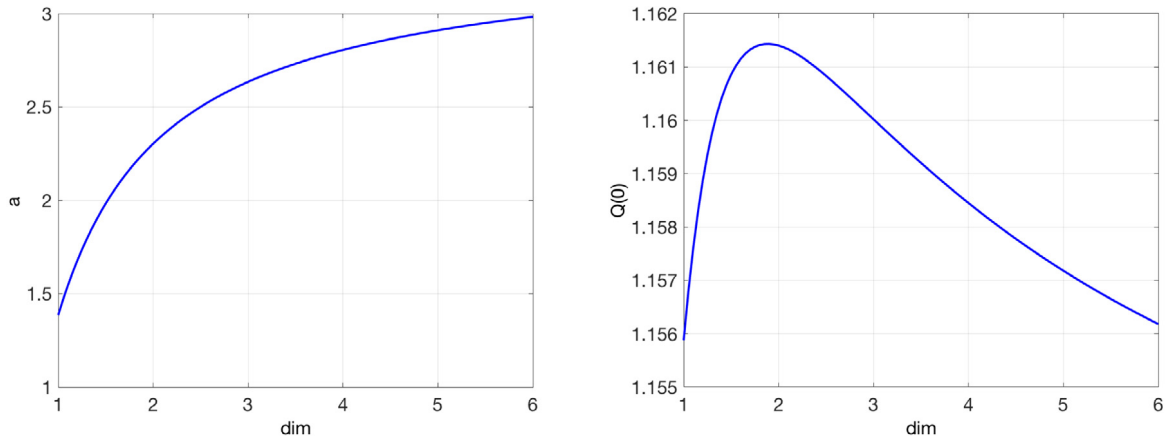


Fig. 7. The change of  $a$  and  $Q(0) = Q_{1,0}(0)$  with respect to the dimension  $d$  for the septic case ( $\sigma = 3$ ).

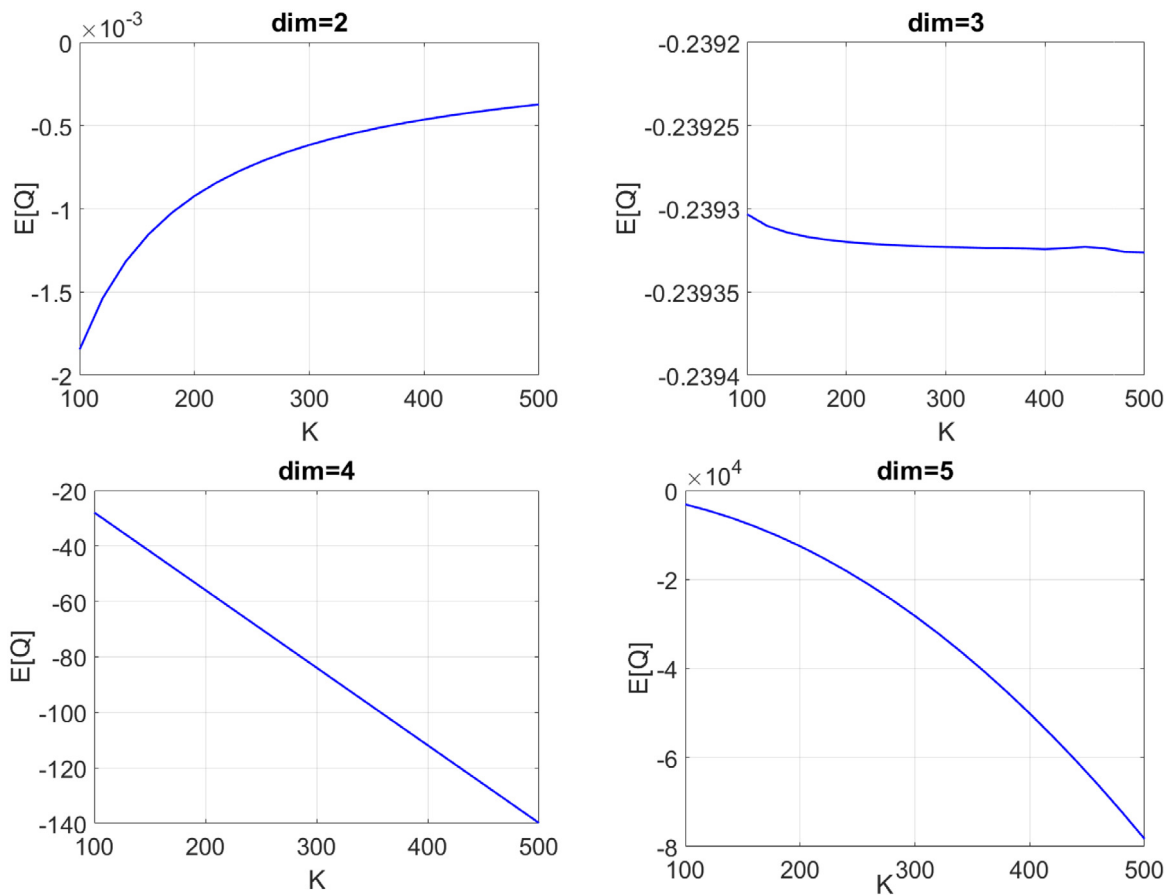


Fig. 8. The change of the energy with respect to the computational interval  $K$  in dimension  $d = 2, 3, 4, 5$  for the quintic case ( $\sigma = 2$ ).

**Proof.** Eq. (2.1) is equivalent to the following Volterra integral equations. For  $d = 2$ :

$$\begin{cases} Q(\xi) = Q(0) - ia \int_0^\xi sQ(s)ds \\ \quad + \int_0^\xi \left[ 1 + ia\left(2 - \frac{1}{\sigma}\right) - |Q(s)|^{2\sigma} \right] \\ \quad \times Q(s) [s(\ln \xi - \ln s)] ds, \\ Q(\infty) = 0. \end{cases} \quad (2.9)$$

For  $d > 2$ :

$$\begin{cases} Q(\xi) = Q(0) - ia \int_0^\xi sQ(s)ds \\ \quad + \frac{1}{d-2} \int_0^\xi \left[ 1 + ia\left(d - \frac{1}{\sigma}\right) - |Q(s)|^{2\sigma} \right] \\ \quad \times Q(s) \left( s - \frac{s^{d-1}}{\xi^{d-2}} \right) ds, \\ Q(\infty) = 0. \end{cases} \quad (2.10)$$

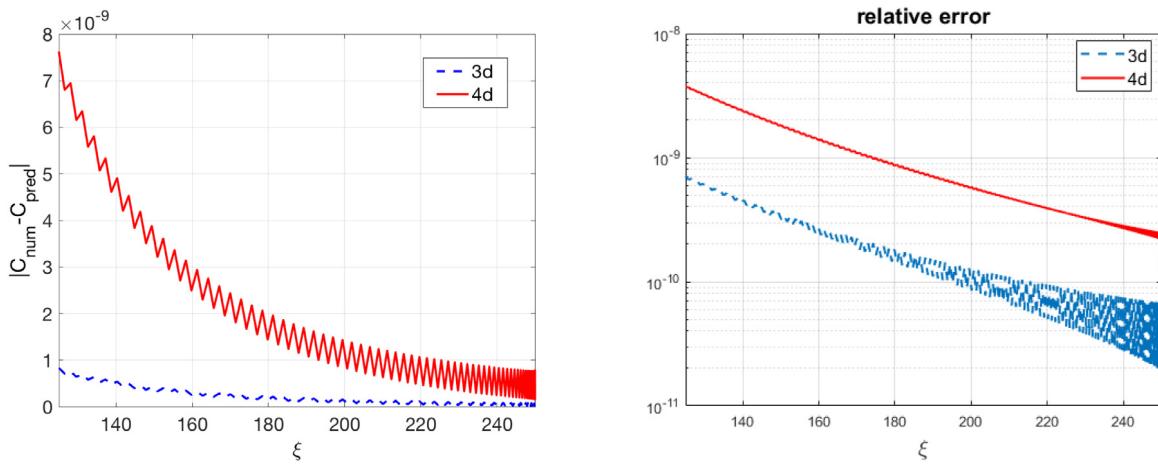


**Fig. 9.** Left:  $|C_{\text{num}} - C_{\text{pred}}|$  for the 3d (blue solid line) and the 4d (red dash line) energy-critical cases. One can see that both errors are on the order of  $10^{-9}$ . Right: relative error  $|C_{\text{num}}/C_{\text{pred}} - 1|$  of the above quantities.

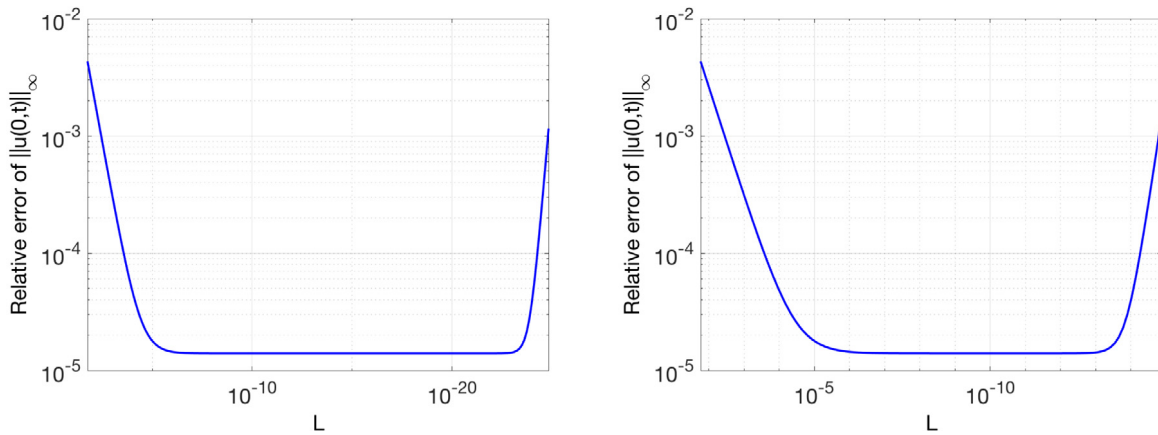


**Fig. 10.** The relative error between the predicted blow-up rate and the numerical results for the 2d quintic case. The increase of the error at a very small  $L$  is due to less accurate estimate of the blow-up time  $T$ .

Both of Eqs. (2.9) and (2.10) are of the form

$$Q(\xi) = Q(0) + \int_0^\xi g(s, \xi, Q(s)) ds, \quad Q(\infty) = 0. \quad (2.11)$$

By Lemmas 2.4 and 2.5 (arguing similarly to [27]), one can easily see that (2.11) has a continuous unique solution on the interval  $\xi \in [0, M]$  for a fixed  $M > 0$  as  $g(s, \xi, Q(s))$  is continuous. Both existence and uniqueness are extended to  $M = \infty$  by Lemma 2.6 as  $|Q(\xi)|$  is bounded on any finite interval  $[0, M]$ . We next note that  $Q$  is the solution not only to Eq. (2.9), or (2.10), but actually to the differential equation (2.1), and thus, differentiating  $Q$  twice classically, it is straightforward to see that  $Q$  is of class  $C^2$ , which finishes the proof.  $\square$

**Corollary 2.7.** For  $d \geq 2$  and  $s_c > 0$ , if  $\sigma = 1$ , then  $|Q(\xi)| \lesssim \xi^{-1}$  for  $\xi$  large enough (recall that  $\xi$  is radial variable here, and thus, non-negative).

**Proof.** When  $\sigma = 1$ , the term  $2a(\frac{1}{\sigma} - 1) \int_0^\xi s|Q|^2 ds$  in (2.3) cancels. Then, the rest of the proof is the same as in [27, Theorem 2.2].  $\square$

**2.2. Decay of  $Q$  and an alternative proof of existence for the case  $s_c = \frac{1}{2}$**

The argument of Theorem 2.1 does not provide information on the decay rate of  $Q$  except for  $\sigma = 1$  as in Corollary 2.7 (though

the asymptotic analysis in [24] showed it should be  $|\xi|^{-\frac{1}{\sigma}}$ , and the argument for the cubic nonlinearity from [27] also gave the decay rate  $|\xi|^{-1}$  as we showed above). An argument of X.-P. Wang from [26] allows us to obtain extension of the existence theory of  $Q$  to other  $s_c > 0$  with  $\sigma > \frac{1}{2}$  as well as the decay properties, which we state in Theorem 2.2. We note that this theorem should hold for all  $s_c > 0$  but for brevity we present the argument for  $s_c = \frac{1}{2}$ , see also our Remark 2.8 on how to handle other cases. This alternative approach implies that  $|Q(\xi)| \leq |\xi|^{-\frac{1}{\sigma}}$ , the same conclusion as in the asymptotic analysis in [24].

**Theorem 2.2.** For any  $a > 0$  satisfying  $s_c = \frac{1}{2}$  and  $\sigma > \frac{1}{2}$ , there exists a global nontrivial solution of (2.1) such that  $Q(\xi) = \frac{1}{\xi^{\frac{1}{\sigma}}} R(\xi)$ , where  $R(\xi)$  is bounded.

**Proof.** In order to apply the fixed point argument, we first define the Banach space

$$\mathbb{B} = \left\{ y(t) | y(t) \in C^1[0, \infty), |y(t)|, \frac{|y'(t)|}{t+1} \text{ bounded}, y(0) = (0, 0)^T \right\}$$

with the norm

$$\|y(t)\|_{\mathbb{B}} = \max \left\{ \sup_{t \in [0, \infty)} |y(t)|, \sup_{t \in [0, \infty)} \frac{|y'(t)|}{t+1} \right\}.$$

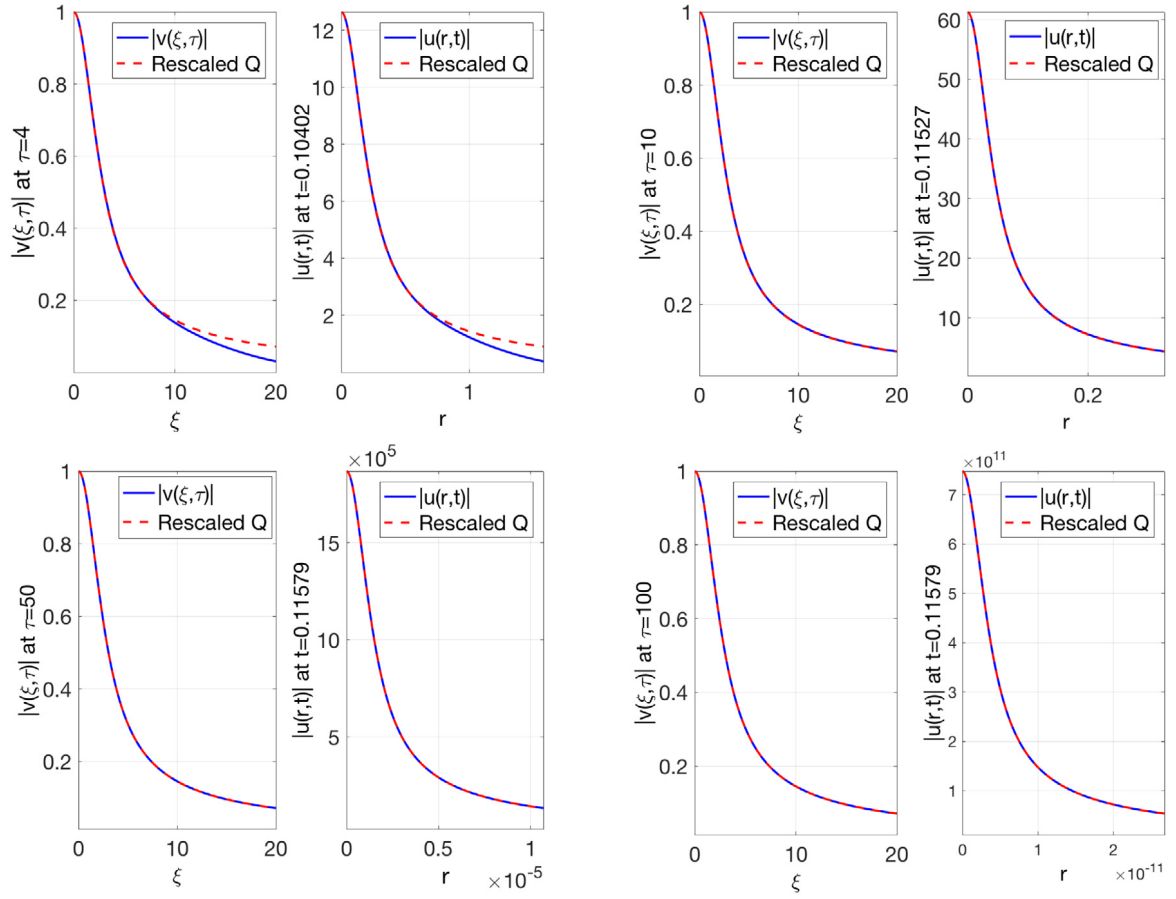


Fig. 11. Blow-up profiles for the 3d cubic case at different times  $\tau$  and  $t$ .

We go back to Eq. (2.1). We rescale the solution  $Q$  as

$$\tilde{Q}(t) = \frac{1}{a^{1/2\sigma}} Q\left(\frac{t}{a^{1/2}}\right). \quad (2.12)$$

Then Eq. (2.1) becomes

$$\tilde{Q}_{tt} + \frac{d-1}{t} \tilde{Q}_t - \frac{1}{a} \tilde{Q} + i(t \tilde{Q}_t + \frac{\tilde{Q}}{\sigma}) + |\tilde{Q}|^{2\sigma} \tilde{Q} = 0. \quad (2.13)$$

Further substitution

$$\tilde{Q}(t) = \frac{1}{t^{1/\sigma}} e^{-it^2/4} P(t),$$

and recalling  $s_c = \frac{d}{2} - \frac{1}{\sigma}$ , transforms Eq. (2.13) into

$$P_{tt} + \frac{2s_c - 1}{t} P_t + \frac{1}{\sigma} \left(2 + \frac{1}{\sigma} - d\right) \frac{1}{t^2} P - \frac{1}{a} P + \frac{t^2}{4} P - is_c P + \frac{|P|^{2\sigma} P}{t^2} = 0. \quad (2.14)$$

The term  $\frac{2s_c - 1}{t} P_t$  is eliminated by taking  $s_c = \frac{1}{2}$ . By splitting  $P = x_1 + ix_2$ , where  $x_1$  and  $x_2$  are real and  $x = (x_1, x_2)^T$ , and rewriting (2.14) as a first order system by letting  $X = (x(t), x_t(t))^T$ , we obtain

$$\begin{cases} X' = A(t)X + H_y(t)X \\ X(0) = (0, 0, b, 0)^T, \end{cases} \quad (2.15)$$

where  $b$  is some constant, and

$$A(t) = \begin{bmatrix} 0 & I \\ -a(t)I + \frac{1}{2}J & 0 \end{bmatrix}, \quad H_y(t) = \begin{bmatrix} 0 & 0 \\ \frac{|x(t)|^{2\sigma}}{t^2} I & 0 \end{bmatrix}, \quad (2.16)$$

$$a(t) = \frac{t^2}{4} - \frac{1}{a} + \frac{1}{\sigma} \left(\frac{3}{2} - \frac{d}{2}\right) \frac{1}{t^2}, \quad J = \begin{bmatrix} 0 & -1 \\ 1 & 0 \end{bmatrix},$$

and  $I$  is the  $2 \times 2$  identity matrix.

From (2.16), we observe that the linear part  $A(t)$  is of the same form as in [26], except with the extra term  $\frac{1}{\sigma}(\frac{3}{2} - \frac{d}{2})\frac{1}{t^2}$  in  $a(t)$ , which is of the higher order and can be neglected in the analysis. Therefore, the uniform bound on the linear term  $A(t)$  is obtained according to the argument in [26, Section 3 and Section 4, Chapter 2].

**Remark 2.8.** The statement of Theorem 2.2 holds for other  $s_c \neq \frac{1}{2}$ , which can be obtained as follows: if  $s_c \neq \frac{1}{2}$ , then the matrix  $A(t)$  in (2.16) becomes

$$A(t) = \begin{bmatrix} 0 & I \\ -a(t)I + \frac{1}{2}J & \frac{1 - 2s_c}{\xi} I \end{bmatrix}.$$

Consequently, the four eigenvalues of the matrix  $A(t)$  are

$$\begin{aligned} \lambda_1 &= \sqrt{-a + \frac{i}{2} - 2s_c} + 1, & \lambda_2 &= \sqrt{-a - \frac{i}{2} - 2s_c} + 1, \\ \lambda_3 &= -\sqrt{-a + \frac{i}{2} - 2s_c} + 1, & \lambda_4 &= -\sqrt{-a - \frac{i}{2} - 2s_c} + 1. \end{aligned}$$

Next, after some tedious computations, we get the corresponding eigenfunctions, then diagonalizing the matrix  $A(t)$  yields a

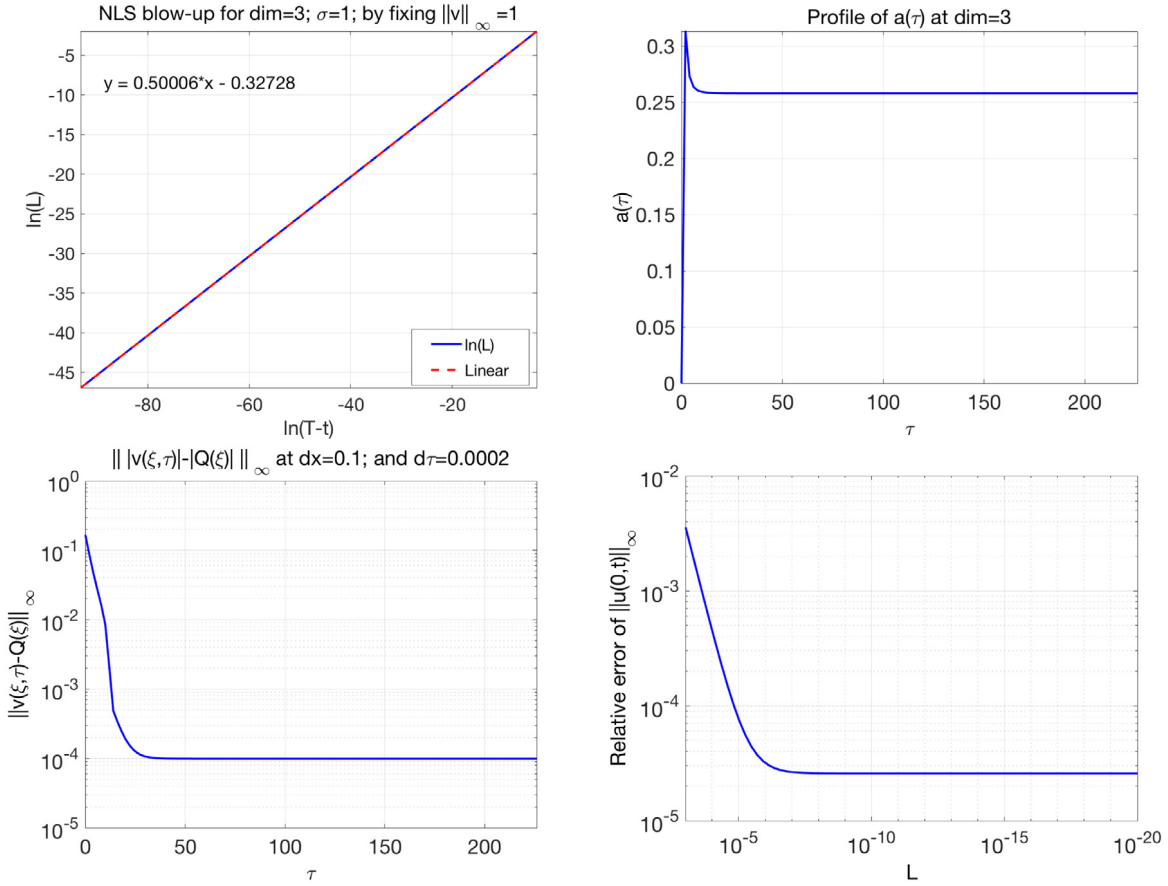


**Fig. 12.** Blow-up data for the 3d cubic case:  $\ln(T-t)$  vs.  $\ln(L)$  (upper left), the quantity  $a(\tau)$  (upper right), the distance between  $Q$  and  $v$  on time  $\tau$  ( $\|v(\tau) - Q\|_{L^\infty}$ ) (lower left), the relative error with respect to the predicted blow-up rate (lower right).

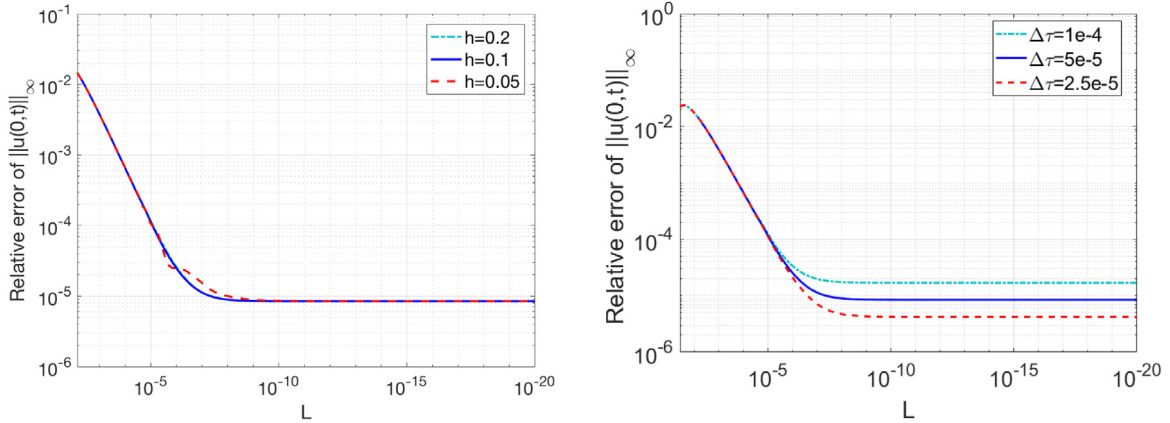


**Fig. 13.** The relative error comparison when choosing different step sizes in space and time for the 3d quintic ( $\sigma = 2$ ) case.

corresponding expression to (2.16) and neglecting higher orders finishes this argument in a general case.

Continuing with the proof of the theorem, we follow the same process as in [26, Chapter 2]: it is easy to see that for Lemma 2 in [26, Section 4, Chapter 2], the prior bound for the nonlinear term  $\tilde{B}_y(t)$ , which comes from a series of linear transformations on  $H_y(t)$  (see [26, Section 3, Chapter 2]), turns out to be  $\|\tilde{B}_y(t)\|_{\mathbb{B}} \leq \frac{1}{t^\alpha}$  for large  $t$ , where  $\alpha = \min\{3, 2\sigma + 1\}$ . In order to apply the Gronwall's inequality for Lemma 3 in [26, Section 4, Chapter 2] for the next step, we need  $2\sigma + 1 < 2$ . Thus, we need  $\sigma > \frac{1}{2}$ .

The proof of Theorem 2.2 is completed by an application of the Schauder fixed point theorem. The rest of the details can be found in [26, Section 4, Chapter 2].  $\square$

**Remark 2.9.** Note that the above Theorems 2.1 and 2.2 do not guarantee that for any  $a > 0$ , the solution  $Q$  would be slowly decaying, i.e.,  $Q = \alpha Q_1 + \beta Q_2$  with  $\beta = 0$ , where  $Q_1$  and  $Q_2$  are as in (3.4) in Section 3. This unique solution  $Q$  may include the fast oscillating tails from  $Q_2$  part, which is not suitable for us (due to zero Hamiltonian). The main issue is to identify for which  $a > 0$ , solutions  $Q$  do not have fast oscillating parts, which we start addressing in the next section.

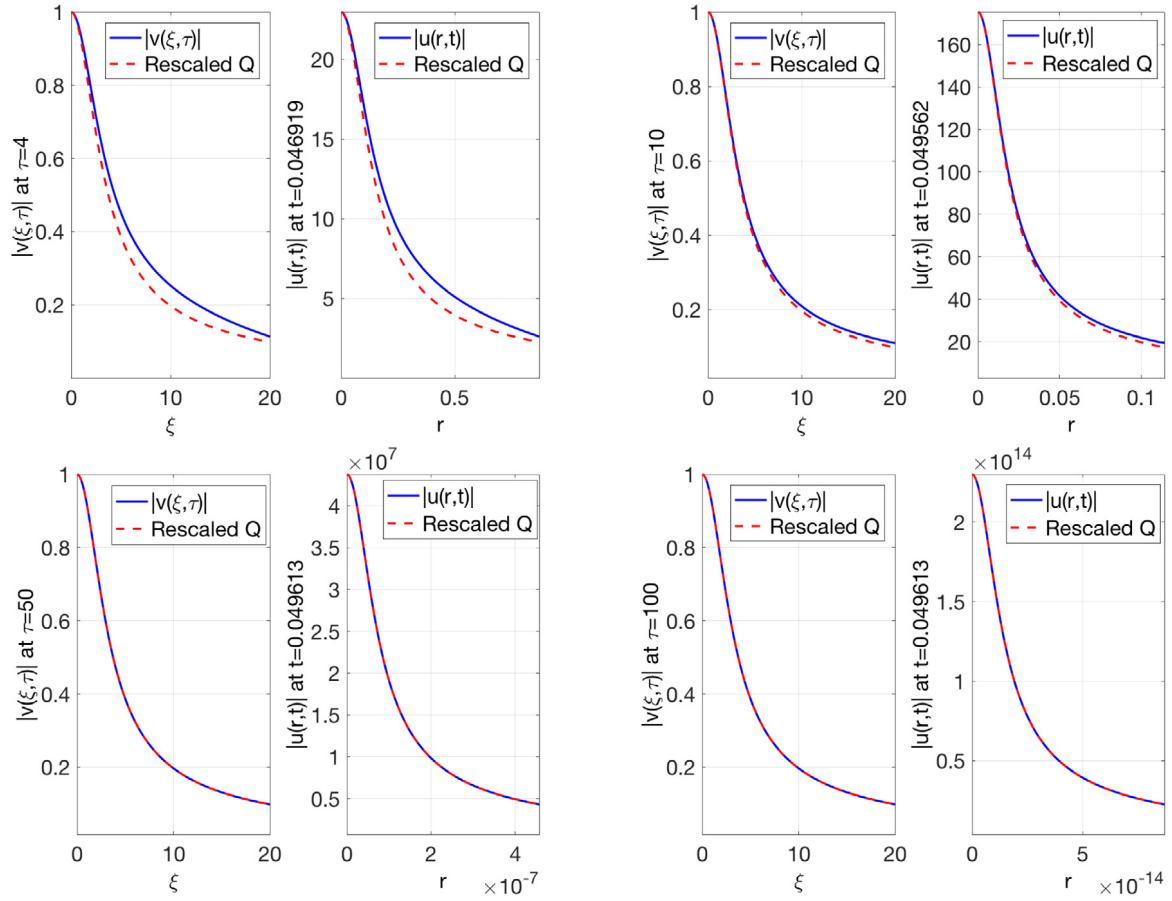


Fig. 14. Blow-up profiles for the 4d cubic case at different time  $\tau$  and  $t$ .

### 3. Profiles $Q$

Observe that after rescaling (1.7), we have the mass and energy in terms of  $v$  as

$$M[v] = L(t)^{2s_c} \int_{\mathbb{R}^d} |v|^2 dx, \quad (3.1)$$

$$E[v] = L(t)^{2s_c-2} \frac{1}{2} \int_{\mathbb{R}^d} \left( |\nabla v|^2 - \frac{2}{p+1} |v|^{p+1} \right) dx \quad (3.2)$$

$$\stackrel{\text{def}}{=} \frac{\omega_d}{2} L(t)^{2s_c-2} H[v].$$

It was shown in [27], see also [29], that in the cubic NLS case (and  $2 < d < 4$ , or equivalently,  $0 < s_c < 1$ ), the Hamiltonian  $H[Q] = 0$  if and only if

$$\left| \left( \frac{1}{\sigma} + \frac{i}{a} \right) Q(\xi) + \xi Q_\xi(\xi) \right| \rightarrow 0 \quad \text{as } |\xi| \rightarrow \infty. \quad (3.3)$$

We note that this property is an essential ingredient in numerical study of solutions to (1.9), since it is a good approximation for the boundary condition  $Q(\infty) = 0$  by taking  $\xi = K$  in (3.3) for some  $K$  large enough (e.g.,  $K = 200$ ).

We next investigate suitable boundary conditions in the case  $s_c \geq 1$ . Recall that the asymptotic analysis in [22] for Eq. (2.1) shows that one can drop the (higher order) nonlinear term  $|Q|^{2\sigma}Q$  in (1.9) and obtain  $Q$  as a linear span of two linearly independent solutions

$$Q_1 \sim |\xi|^{-\frac{i}{a}-\frac{1}{\sigma}}, \quad Q_2 \sim e^{-\frac{ia\xi^2}{2}} |\xi|^{\frac{i}{a}-d+\frac{1}{\sigma}}, \quad (3.4)$$

and hence,  $Q = \alpha Q_1 + \beta Q_2$ . As discussed in the introduction, we exclude the fast oscillating solution  $Q_2$ , since only  $Q_1$  with

the slow decaying tails would produce potential candidates for the stable blow-up profile in the NLS equation (see [5,14] for further details). Note that if  $Q \sim Q_1$ , then the decay of  $Q$  is  $|\xi|^{-\frac{1}{\sigma}}$ , as we also show in Theorem 2.2. Computing  $H[Q]$ , we note that both terms do not converge in the energy-supercritical case (the asymptotic behavior is  $\xi^{2(s_c-1)}$  as  $\xi \rightarrow \infty$ ) and give some constant when  $s_c = 1$ , see exact computation at the end of this section. Therefore, we no longer have the zero Hamiltonian property for  $Q$  when  $s_c \geq 1$ , however, Eq. (3.3) is still a good approximation for the boundary condition  $Q(\infty) = 0$ , since the solution  $Q$  must be linearly dependent on  $Q_1$  when  $\xi \rightarrow \infty$ ; therefore, computing the Wronskian for  $Q$  and  $Q_1$ , gives us

$$\left( \frac{1}{\sigma} + \frac{i}{a} \right) Q(\xi) + \xi Q_\xi(\xi) = 0 \quad \text{as } \xi \rightarrow \infty,$$

which yields (3.3) in all cases  $s_c > 0$ . Thus, we approximate the boundary condition  $Q(\infty) = 0$  by

$$\left( \frac{1}{\sigma} + \frac{i}{a} \right) Q(K) + K Q_\xi(K) = 0, \quad (3.5)$$

taking sufficiently large  $K$ .

We are now ready to compute the profiles for the mass-supercritical cases, including energy-critical and energy-supercritical regimes. We first confirm the results of Budd et al. in [27] (in particular, we show our computations in the 3d cubic case ( $d = 3, \sigma = 1$ ) as the computational consistency check), and then show the results for other nonlinear powers such as  $p = 5$  and  $p = 7$  (or  $\sigma = 2, 3$ , correspondingly) and dimensions  $d = 2, 3, 4, 5$ .

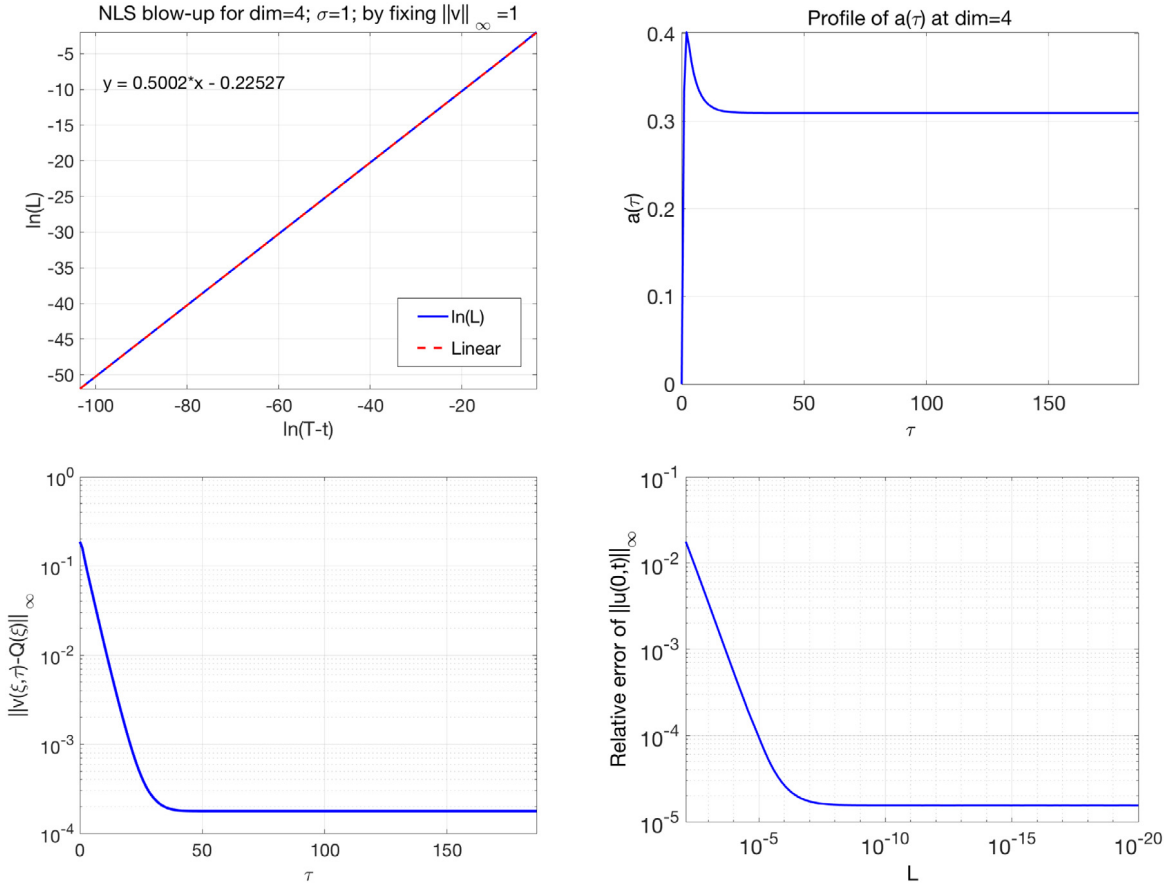


**Fig. 15.** Blow-up data for the 4d cubic case:  $\ln(T-t)$  vs.  $\ln(L)$  (upper left), the quantity  $a(\tau)$  (upper right), the distance between  $Q$  and  $v$  on time  $\tau$  ( $\|v(\tau)-Q\|_{t_\xi^\infty}$ ) (lower left), the relative error with respect to the predicted blow-up rate (lower right).

### 3.1. Computation of $Q$

We split the solution  $Q$  into the real and imaginary parts  $Q = P + iW$ . Then, Eqs. (2.1) and (3.5) become

$$\begin{cases} \Delta P - P - a\left(\frac{W}{\sigma} + \xi W_\xi\right) + (P^2 + W^2)^\sigma P = 0, \\ \Delta W - W + a\left(\frac{P}{\sigma} + \xi P_\xi\right) + (P^2 + W^2)^\sigma W = 0, \\ P_\xi(0) = 0, \\ W(0) = 0, \\ W_\xi(0) = 0, \\ \frac{1}{\sigma}P - \frac{1}{a}W + KP_\xi = 0, \\ \frac{1}{a}P + \frac{1}{\sigma}W + KW_\xi = 0. \end{cases} \quad (3.6)$$

The equation system (3.6) is discretized by the Chebyshev collocation points and differential matrices (see [37,38]). Then, it reduces into the nonlinear algebraic system which can be solved by the matlab solver `fsolve`. The initial guess for the solver `fsolve` for such case is obtained by solving the initial value problem of (2.1) by the matlab solver `ode45`, with the estimation of the parameters  $a$  and  $P(0)$ . This method requires a relative accurate estimation on the values of  $a$  and  $P(0)$ . However, since we know that  $a \approx 0.917$  and  $P(0) \approx 1.885$  for  $\sigma = 1$  from [14,27], the estimation on  $a$  and  $P(0)$  for the other cases can be obtained by *continuous parameter search*. For example, if we want to compute the 4d cubic case ( $d = 4$  and  $\sigma = 1$ ), we use the values of  $a$  and  $P(0)$  to compute the initial guess of  $d = 3.1$ ,

and then compute the solution  $Q$  for  $d = 3.1$ . Next, we use these parameters of  $a$  and  $P(0)$  to compute the case for  $d = 3.2$ , and finally until  $d = 4$ . During our computation, this estimation can be refined by extrapolation, e.g.,  $a|_{d=4} = 3a|_{d=3.9} - 3a|_{d=3.8} + a|_{d=3.7}$ . This refinement allows us to take larger steps on the dimension or nonlinearity and also reduce the iterations in the `fsolve` in the next stage.

We use  $N = 257$  Chebyshev collocation points and take the length of the computational interval  $L_D = 200$  during our computation. The tolerance on `fsolve` is set to be  $10^{-15}$ . For most of the cases, the residue for the algebraic system is on the order of  $10^{-12}$ .

### 3.2. Numerical results on profiles $Q$

We first show our results of  $Q$  solutions in the 3d cubic case (see Fig. 2), where we plot  $|Q|$  (since  $Q$  is complex-valued). Our challenge is to select the initial condition  $Q(0)$  and the parameter  $a$  that yields the slowly oscillating type  $Q_1$  solutions of the profile equation. In [27] it was done by considering the perturbations on the dimension ( $d = 2.0001, 2.001, 2.01$ , etc.) and showing that (at least some)  $Q_1$ -type solutions of the profile equation can be organized in branches of multi-bump solutions  $Q_{K,J}$ .

In these multi-bump solutions  $Q_{K,J}$  the index  $K = 0, 1, 2, \dots$  indicates the branch of the sequence. In the cubic NLS case in [32] it was shown that solutions of each specific branch  $K$  converge non-uniformly as  $d \rightarrow 2$  to the  $H^1$  solution  $Q^K$  of the ‘ground state’ equation (1.5) (here,  $Q^0 \equiv 0$ ,  $Q^1$  is the ground state,  $Q^l$ ,  $l \geq 2$ , are the excited, sign-changing, states). Thus, we are mostly interested in the branch  $K = 1$ , or  $\{Q_{1,J}\}$ , solutions of which non-uniformly converge to the well-known ground state. Solutions

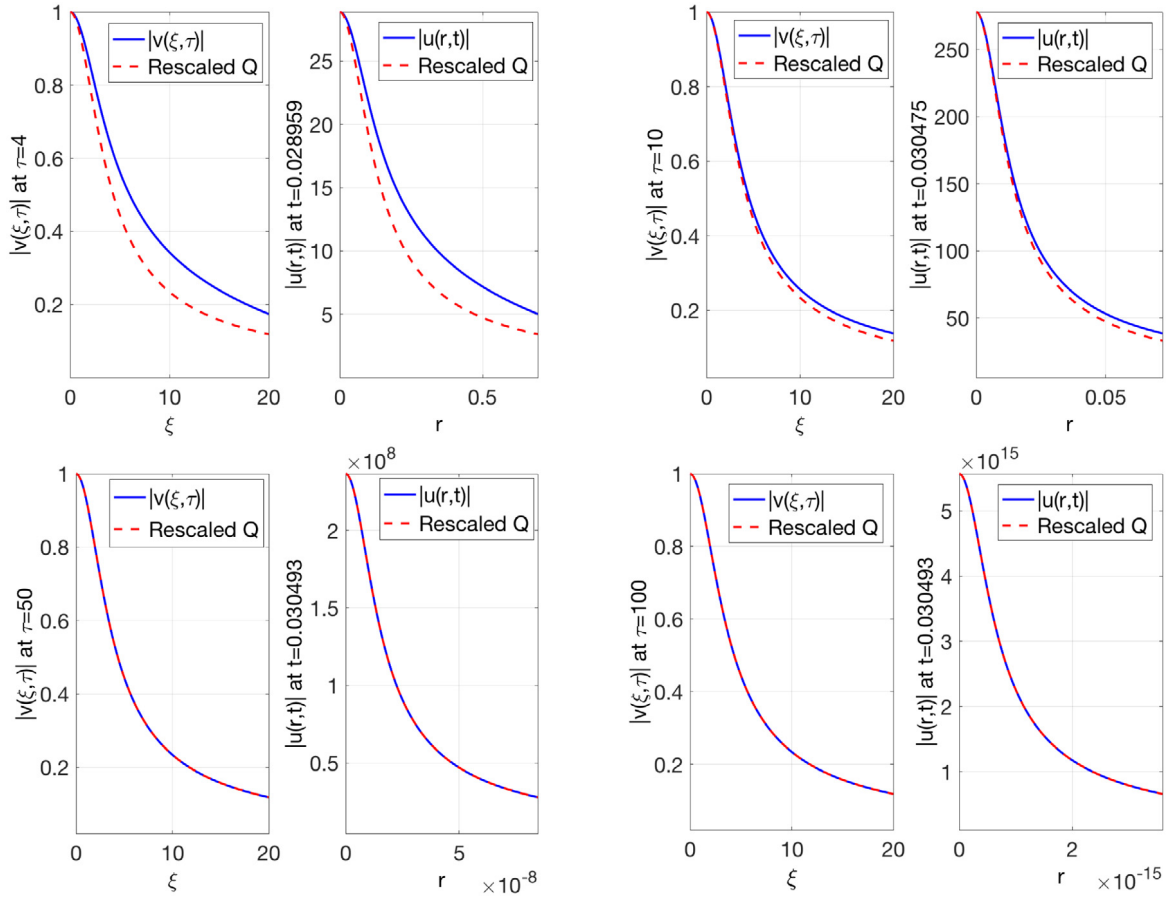


Fig. 16. Blow-up profiles for the 5d cubic case at different time  $\tau$  and  $t$ .

within the branch were classified in [27] (in the cubic NLS case) by the number of bumps (or maxima) in each sequence,  $J = 0, 1, \dots$ , when the dimension  $d$  was close to 2. It was also shown that when  $d$  is close to 2, the number  $K + J$  indicated the number of turning points (as well as maxima) change for a fixed  $J$ , and some profiles of  $|Q|$  lose some turning points, and some even become completely monotone (with no bumps), see Figs. 2–4; in any case, here we keep the notation  $Q_{K,J}$  for consistency.

We obtain  $Q_{1,0}$  from initial guess for parameters  $a$  and  $Q(0)$  in the 3d cubic case we extracted from the literature [14,27] – see the blue curve in Fig. 2; this confirms matching of our computations with previous results. By using another initial guess for parameters  $a$  and  $Q(0)$ , for example, from [27], we obtain the solution  $Q_{1,1}$ , which is the first bifurcation from  $Q_{1,0}$  (see the red dashed curve in Fig. 2).

To really understand the dependence of solutions on parameters  $a$  and  $Q(0)$ , we study the pseudo-phase plane, which was introduced by Kopell–Landman in [29] and adopted in Budd–Chen–Russell [27]. We write

$$Q \equiv C(\xi) \exp\left(i \int_0^\xi \psi\right), \quad D(\xi) = C_\xi / C \equiv \operatorname{Re}(Q_\xi / Q). \quad (3.7)$$

In other words,  $C$  is the amplitude of  $Q$ ,  $C(\xi) = |Q(\xi)|$ ,  $D$  is its logarithmic derivative, and  $\psi$  is the gradient of the phase. In the coordinates  $(C, D)$  we will track the behavior of the graph as it is decreasing down to the origin as both  $C$  and  $D$  approach zero when  $\xi \rightarrow \infty$ . To see that recall that asymptotically

$$Q(\xi) \sim \alpha \xi^{-\frac{1}{\sigma}} \exp\left(-\frac{i}{a} \log(\xi)\right) + \beta \xi^{-(d-\frac{1}{\sigma})}$$

$$\times \exp\left(-\frac{ia\xi^2}{2} + \frac{i}{a} \log(\xi)\right),$$

where the first term is slowly decaying and the second term decays faster with fast oscillations. The solution  $Q$  that varies slowly at infinity, would have no oscillations at the end of the curve (as  $C \rightarrow 0$ ), since

$$C \sim \frac{\alpha}{\xi^{\frac{1}{\sigma}}} \quad \text{and} \quad D \sim -\frac{1}{\sigma \xi} \quad \text{as} \quad \xi \rightarrow \infty.$$

Thus, such solutions will approach the origin in coordinates  $(C, D)$  along the curve  $D \sim -\frac{1}{\sigma \alpha \sigma} C^\sigma$ . In the case of  $\sigma = 1$  (cubic power), this will be a straight line with slope  $-1/\alpha$ , which we demonstrate in the paths shown in Fig. 2 (right plot). In the case of  $\sigma = 2, 3$ , this will be a parabola (quadratic or cubic, respectively), which we show in Figs. 3 and 4 (plots on the right).

If the solution  $Q$  oscillates fast at infinity, then its graph in the coordinates  $(C, D)$  will approach the origin in the oscillating manner, since

$$C \sim \frac{\alpha}{\xi^{\frac{1}{\sigma}}} \quad \text{and} \quad D \sim -\frac{\beta a}{\alpha} \frac{1}{\xi^{d-\frac{2}{\sigma}-1}} \sin\left(\frac{a\xi^2}{2} - \frac{2}{a} \log(\xi)\right).$$

We show an example of such oscillating behavior for  $\sigma = 1$  (cubic nonlinearity in 3d) in Fig. 1, where we perturb the value of  $a$ , while keeping  $Q(0)$  fixed (recall  $Q(0) = Q_{1,0}(0) = 1.8856569903$ ): taking  $a = 0.8$  (left plot) and  $a = 1$  (right plot). Both plots show severe oscillations as the curve approaches the origin (recall that for  $a \approx 0.9$ , or more precise,  $a = 0.9173561446$ , the curve has no oscillations as shown in Fig. 2). We note that our results in Fig. 2 match the ones obtained in [27]

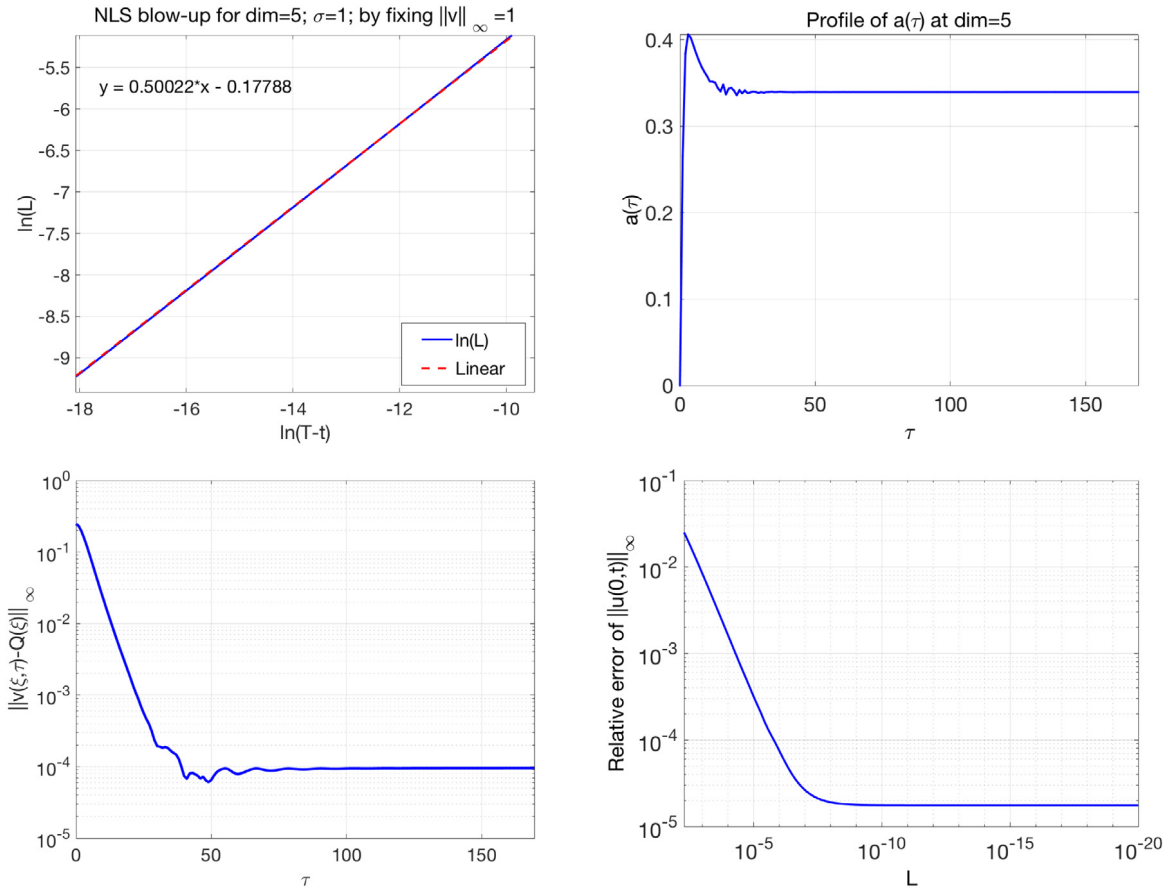


**Fig. 17.** Blow-up data for the 5d cubic case:  $\ln(T-t)$  vs.  $\ln(L)$  (upper left), the quantity  $a(\tau)$  (upper right), the distance between  $Q$  and  $v$  on time  $\tau$  ( $\|v(\tau) - Q\|_{L^\infty}$ ) (lower left), the relative error with respect to the predicted blow-up rate (lower right).

both in the amplitude and phase plane representations, therefore, we conclude that our numerical approach is trustful.

In Figs. 3–4 we show  $|Q|$  profiles for the 3d quintic ( $d = 3$  and  $\sigma = 2$ ) and 3d septic ( $d = 3$  and  $\sigma = 3$ ) cases, which are the energy-critical and energy-supercritical cases, respectively.

We next investigate how the values  $Q(0) \stackrel{\text{def}}{=} Q_{1,0}(0)$  and  $a$  change with respect to the dimension  $d$ . The results are shown in Fig. 5 (cubic), Fig. 6 (quintic) and Fig. 7 (septic). Observe that both values produce a smooth curve from the energy-subcritical regime to the energy-supercritical regime.

We next study more closely the values of (conserved) energy depending on the critical scaling index  $s_c$ . Recall that motivated by the scaling invariance, we seek the self-similar blow-up solutions of (1.1) of the form

$$u(r, t) = \frac{1}{(\sqrt{2a(T-t)})^{\frac{1}{\sigma}}} Q\left(\frac{r}{\sqrt{2a(T-t)}}\right) \times \exp\left(i\theta + \frac{i}{2a} \log \frac{T}{T-t}\right). \quad (3.8)$$

The rescaled mass and energy for  $u(r, t)$  in terms of  $Q(\xi)$  are

$$M[u(t)] = C_{a,d}(T-t)^{s_c} \int_0^\infty |Q(\xi)|^2 \xi^{d-1} d\xi, \quad (3.9)$$

$$E[u(t)] = C_{a,d}(T-t)^{s_c-1} \int_0^\infty \left(|Q_\xi|^2 - \frac{1}{\sigma+1} |Q|^{2\sigma+2}\right) \times \xi^{d-1} d\xi = C_{a,d}(T-t)^{s_c-1} H[Q]. \quad (3.10)$$

For  $s_c < 1$ ,  $(T-t)^{s_c-1} \rightarrow \infty$  as  $t \rightarrow T$ . From the energy conservation in (3.10),  $H[Q]$  should be zero, since  $E[u(t)]$  remains

constant in time  $t$ . For  $s_c = 1$ ,  $(T-t)^{s_c-1} = 1$ , and thus,  $H[Q]$  should be a constant. For  $s_c > 1$ ,  $(T-t)^{s_c-1} \rightarrow 0$  as  $t \rightarrow T$ , and thus,

$$\int_0^\xi \left(|Q_\xi|^2 - \frac{1}{\sigma+1} |Q|^{2\sigma+2}\right) \xi^{d-1} d\xi \rightarrow \infty \quad \text{as } \xi \rightarrow \infty.$$

Fig. 8 justifies the above reasoning. We calculate the energy of  $Q$  in the quintic NLS case ( $\sigma = 2$ ) in various dimensions, truncated at different lengths of the interval  $K$ . The top left subplot shows that in the 2d case the energy  $E[Q]$  goes to zero as the interval  $K \rightarrow \infty$ , this is consistent for energy-subcritical setting, here  $s_c = \frac{1}{2} < 1$ . The top right subplot shows that in the 3d case the energy  $E[Q]$  goes to a constant as  $K \rightarrow \infty$ , this is the energy-critical case,  $s_c = 1$ . The bottom left subplot shows that in the 4d case the energy  $E[Q]$  goes to negative infinity linearly as  $K \rightarrow \infty$ , here  $s_c = \frac{3}{2} > 1$ . The bottom right subplot shows that in the 5d case the energy  $E[Q]$  goes to negative infinity quadratically as  $K \rightarrow \infty$ , here  $s_c = 2 > 1$ . Furthermore, the bottom two subplots justify that the solution  $Q$  decays with a rate of  $|Q| \sim \xi^{-1/\sigma}$ , since substituting  $|Q| = \xi^{-1/\sigma}$  into (3.10) and integrating from  $K_0$  to  $\infty$ , one gets

$$E(Q) \sim \int_{K_0}^\infty \xi^{2s_c-3} d\xi.$$

This matches the linear decay for  $s_c = \frac{3}{2}$  (e.g., see  $d = 4$  and  $\sigma = 2$  in Fig. 8), and the quadratic decay for  $s_c = 2$  (e.g., see  $d = 5$  and  $\sigma = 2$  in Fig. 8).

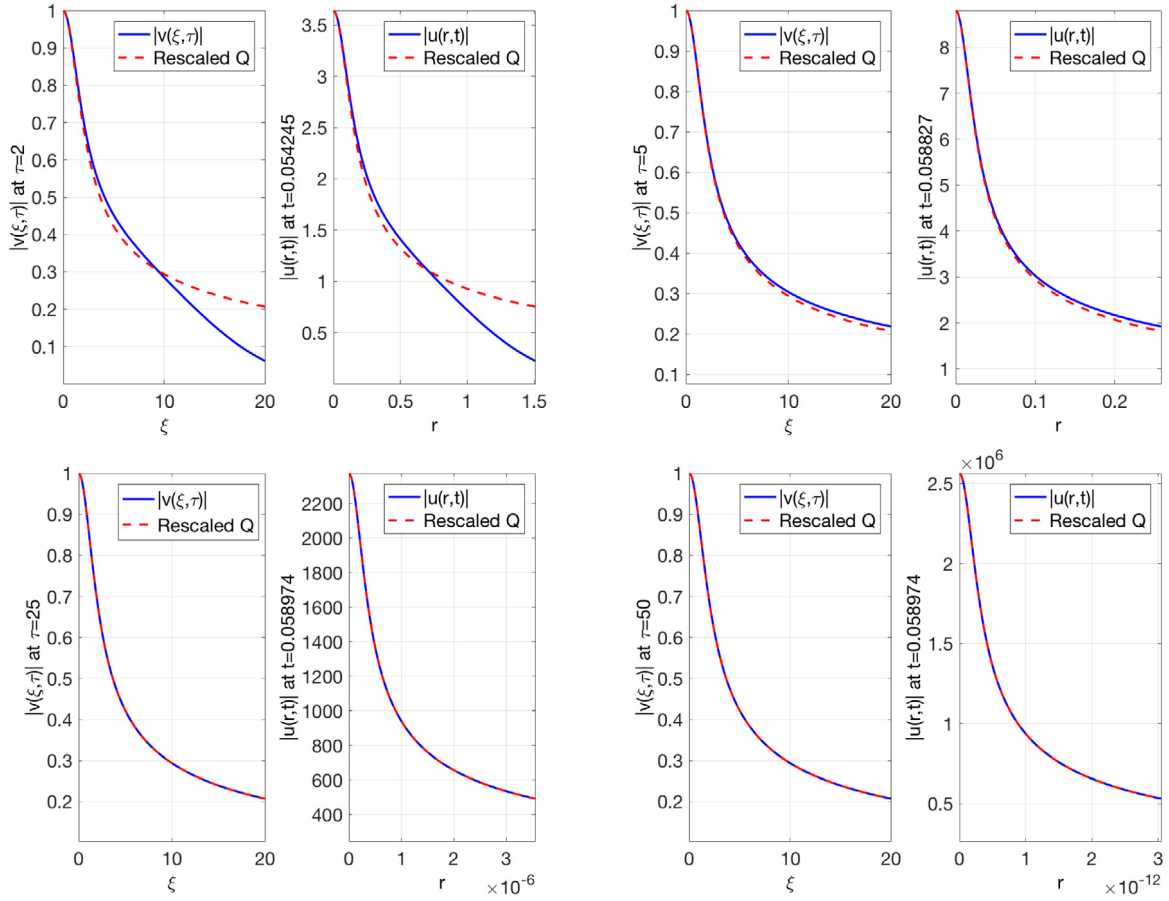


Fig. 18. Blow-up profiles for the 2d quintic case at different time  $\tau$  and  $t$ .

### 3.3. Further justification of the constant Hamiltonian for the energy critical case

The conjecture that  $H[Q] = \text{const}$  for the energy critical case ( $s_c = 1$ ) can be justified by the following argument.

From (3.4) the asymptotic behavior of  $Q$  satisfies  $Q(\xi) \approx C_0 \xi^{-\frac{1}{d-1} - \frac{1}{\sigma}}$  for  $\xi \gg 1$ . Assuming  $H[Q]$  being finite, we have

$$H[Q] = \int_0^{\xi_0} \left( |Q_\xi|^2 - \frac{1}{\sigma+1} |Q|^{2\sigma+2} \right) \xi^{d-1} d\xi + \int_{\xi_0}^{\infty} \left( |Q_\xi|^2 - \frac{1}{\sigma+1} |Q|^{2\sigma+2} \right) \xi^{d-1} d\xi < \infty. \quad (3.11)$$

The first integral of (3.11) gives a constant. Since neither of the terms  $|Q_\xi|^2$  and  $|Q|^{2\sigma+2}$  are integrable, these two terms must cancel each other in the second integral. The direct calculation for the second integral in (3.11) gives

$$C_0 = \left[ (\sigma+1) \left( \frac{1}{\sigma^2} + \frac{1}{a^2} \right) \right]^{\frac{1}{2\sigma}}. \quad (3.12)$$

Fig. 9 shows the difference of  $C_0$  numerically calculated from (3.6) ( $C_0 := C_{\text{num}}$ ) and  $C_0$  calculated from (3.12) ( $C_0 := C_{\text{pred}}$ ). Observe that the difference is on the order of  $10^{-9}$  for  $Q_{1,0}$  in both  $d = 3$  (blue solid line) and  $d = 4$  (red dash line). Moreover, both are decreasing as  $\xi$  is increasing.

Now that we have developed a certain description of profiles  $Q$ , in particular, numerical identification and properties of  $Q_{1,0}$ , we proceed to investigating the dynamics of stable blow-up solutions in the mass-supercritical cases.

## 4. Blow-up dynamics for the NLS equation

### 4.1. Numerical method

We compute the rescaled equation (1.7) and then reconstruct the solution  $u(x, t)$  from the rescaled equation, since the solution  $v(\xi, \tau)$  to the rescaled equation exists globally in time. This method is called the *dynamic rescaling method*, which was first introduced by LeMesurier, Papanicolaou, Sulem and Sulem in [13,22]. This method needs the prior knowledge of the scaling of the singular part of the solution (scaling property).

There are several other methods that can track the blow-up dynamics. For example, one may use the adaptive mesh method in [15], moving mesh method in [27], iterative grid redistribution method in [39] for multi-dimensions and [40] for the 1d case, see also discussion on numerical treatments in [33]. These methods, unlike the dynamic rescaling method, do not need the prior knowledge of the scaling of the singular part and can deal with more general blow-up dynamics cases. Here, however, we consider generic data which leads to the peak-type solutions, i.e., solutions attain their maximum at the origin, see [11, Chapter 14], and the prior knowledge is already given by rescaling. Therefore, the dynamic rescaling method is more effective for our task.

We fix the value  $\|v(\xi, \tau)\|_{L^\infty_\xi} \equiv 1$  in time  $\tau$  as in [24] and [41], and write

$$L(t) = \left( \frac{1}{\|u(t)\|_{L^\infty}} \right)^\sigma, \quad (4.1)$$

and

$$a(\tau) = -\sigma \operatorname{Im} (\bar{v} \Delta v)_{|(0,\tau)}. \quad (4.2)$$

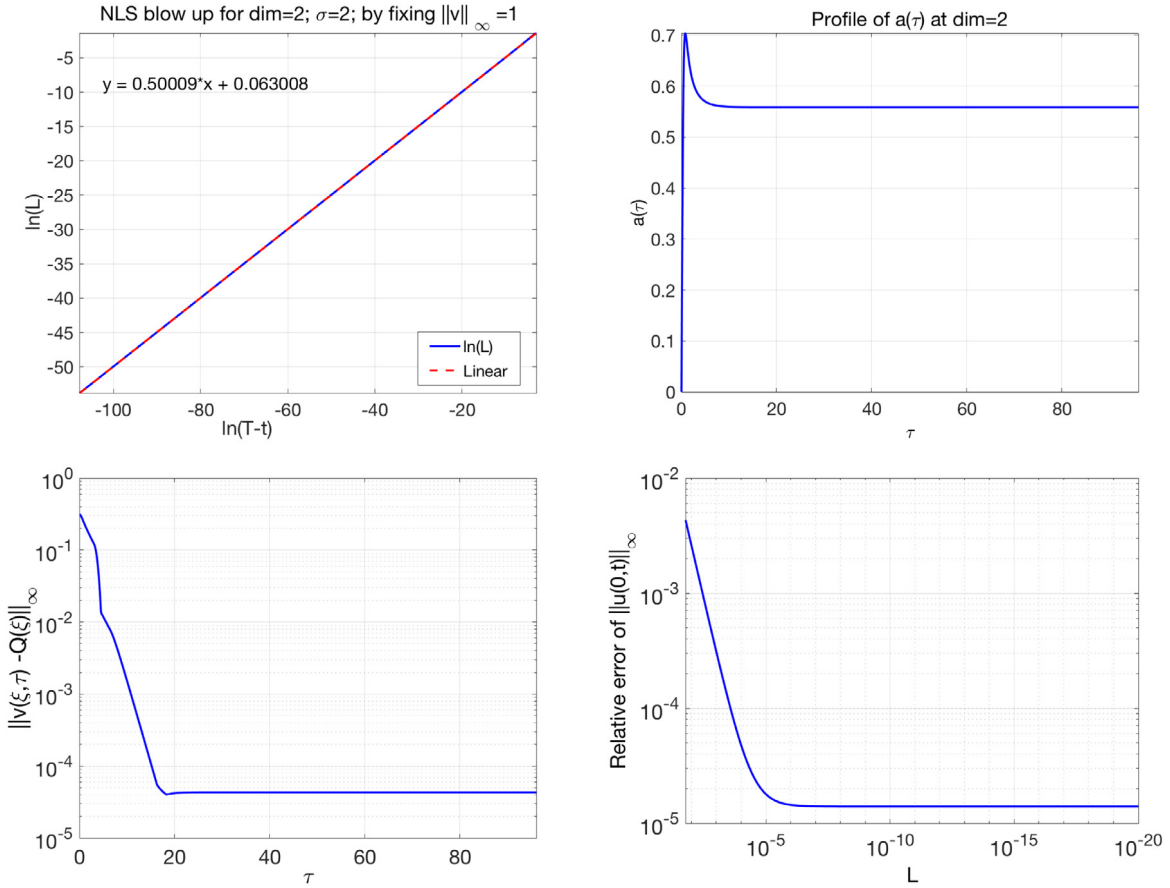


**Fig. 19.** Blow-up data for the 2d quintic case:  $\ln(T-t)$  vs.  $\ln(L)$  (upper left), the quantity  $a(\tau)$  (upper right), the distance between  $Q$  and  $v$  on time  $\tau$  ( $\|v(\tau) - Q\|_{L^\infty}$ ) (lower left), the relative error with respect to the predicted blow-up rate (lower right).

Eq. (1.7) can be written as

$$i v_\tau + \Delta v + \mathcal{N}(v) = 0, \quad \tau \in [0, \infty), \quad \xi \in [0, \infty), \quad (4.3)$$

with

$$\mathcal{N}(v) = ia(\tau) \left( \xi v_\xi + \frac{v}{\sigma} \right) + |v|^{2\sigma} v.$$

The initial value  $v_0(\xi)$  is calculated from (1.6) by setting  $\|v_0\|_{L^\infty} = 1$ .

Let  $N \in \mathbb{Z}$  be a fixed integer,  $[0, L_D]$  the computational domain with  $L_D \gg 1$ , and  $h = \frac{L_D}{N}$  the uniform grid size in space. Let  $v_j \approx v(jh, \tau)$  denote the semi-discrete approximate solution at  $jh, j = 0, 1, \dots, N$ . The spatial derivative is approximated by the sixth order central difference scheme:

$$v_\xi(jh, \tau) \approx D_6^{(1)} v_j = \frac{1}{60h} [-v_{j-3} + 9v_{j-2} - 45v_{j-1} + 45v_{j+1} - 9v_{j+2} + v_{j+3}], \quad (4.4)$$

$$v_{\xi\xi}(jh, \tau) \approx D_6^{(2)} v_j = \frac{1}{180h^2} [2v_{j-3} - 27v_{j-2} + 270v_{j-1} - 490v_j + 270v_{j+1} - 27v_{j+2} + 2v_{j+3}], \quad (4.5)$$

and the Laplacian operator is approximated by

$$\Delta v(jh, \tau) \approx \Delta_h v_j = v_{\xi\xi}(jh, \tau) + \frac{d-1}{jh} v_\xi(jh, \tau). \quad (4.6)$$

When the grid points beyond the right-hand side computational domain are needed, we set up the fictitious points obtained by

extrapolation,

$$v_{N+2} = 8v_{N+1} - 28v_N + 56v_{N-1} - 70v_{N-2} + 56v_{N-3} - 28v_{N-4} + 8v_{N-5} - v_{N-6}.$$

For the grid points beyond the left-hand side computational domain, note that  $v(\xi)$  is radially symmetric, and thus, we use the fictitious points  $v_{-j} = v_j$ . The singularity at  $\xi = 0$  in the Laplacian term  $\Delta_h$  is eliminated by the L'Hospital's rule

$$\lim_{\xi \rightarrow 0} \frac{d-1}{\xi} v_\xi = (d-1)v_{\xi\xi}.$$

The time discretization is similar to our previous work [12] for the mass-critical case (see also in [5]). Let  $\Delta\tau$  denote the uniform time step with respect to the rescaled time  $\tau$  and  $\tau_m = m \cdot \Delta\tau, m = 1, 2, \dots$ . Let  $v_j^{(m)} \approx v(jh, m \cdot \Delta\tau)$  be the approximate solution at  $(jh, m \cdot \Delta\tau)$ , and  $L_m$  the approximation of  $L(\tau_m)$ . The time evolution of (4.3) can be approximated by the second order Crank–Nicolson–Adam–Bashforth method:

$$i \frac{v_j^{(m+1)} - v_j^{(m)}}{\Delta\tau} + \frac{1}{2} \left( \Delta_h v_j^{(m+1)} + \Delta_h v_j^{(m)} \right) + \frac{1}{2} \left( 3\mathcal{N}(v_j^{(m)}) - \mathcal{N}(v_j^{(m-1)}) \right) = 0, \quad (4.7)$$

given the initial condition  $v^{(0)}$  and  $v^{(1)}$ . Here,  $v^{(1)}$  is obtained by the standard second order explicit Runge–Kutta method (RK2). We introduce the two-step Adams predictor–corrector method as in [11, Chapter 28] to increase the accuracy and stability, while

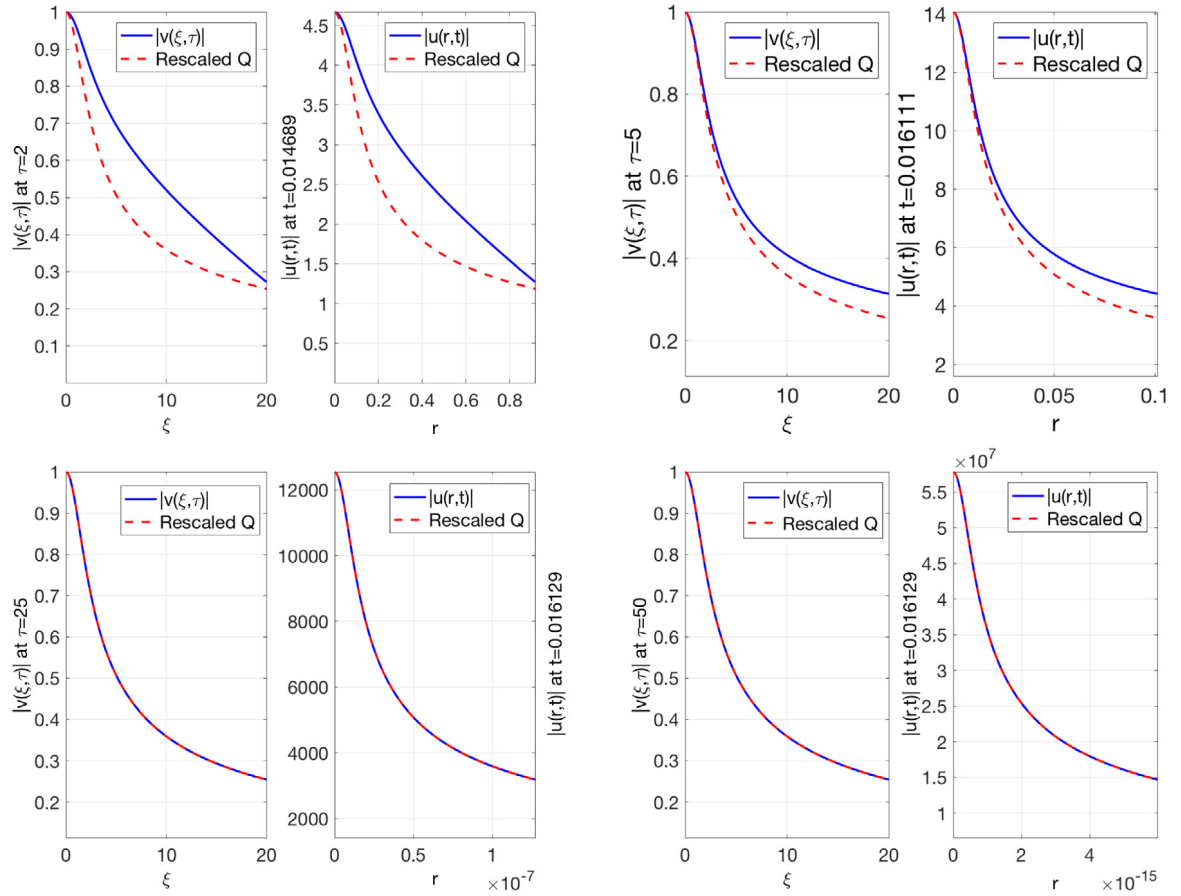


Fig. 20. Blow-up profiles for the 3d quintic case at different time  $\tau$  and  $t$ .

remaining a second order scheme in time:

$$i \frac{v_{\text{pred},j}^{(m+1)} - v_j^{(m)}}{\Delta\tau} + \frac{\Delta_h v_{\text{pred},j}^{(m+1)} + \Delta_h v_j^{(m)}}{2} + \frac{3}{2} \mathcal{N}(v_j^{(m)}) - \frac{1}{2} \mathcal{N}(v_j^{(m-1)}) = 0, \quad (\text{P}) \quad (4.8)$$

$$i \frac{v_j^{(m+1)} - v_j^{(m)}}{\Delta\tau} + \frac{\Delta_h v_j^{(m+1)} + \Delta_h v_j^{(m)}}{2} + \frac{1}{2} \mathcal{N}(v_{\text{pred},j}^{(m+1)}) + \frac{1}{2} \mathcal{N}(v_j^{(m-1)}) = 0. \quad (\text{C}) \quad (4.9)$$

We use the method in [24] to reconstruct the solution in  $(r, t)$  variable. After getting the value  $v^{(m+1)}$ , we update the value  $a^{(m+1)}$  from (4.2). From (1.8),  $\ln L(\tau_{m+1})$  is obtained by the second order trapezoid rule:

$$\ln L(\tau_{m+1}) = \ln L(\tau_m) + \frac{\Delta\tau}{2} (a^{(m+1)} + a^{(m)}). \quad (4.10)$$

Then, we have  $L(\tau_{m+1}) = \exp(\ln L(\tau_{m+1}))$ . Denoting  $\Delta t_{m+1} := \tau_{m+1} - \tau_m$ , we obtain this difference from the last equation of (1.6)

$$\Delta t_{m+1} = \Delta\tau L^2(\tau_{m+1}). \quad (4.11)$$

Thus, the mapping for rescaled time  $\tau$  back to the real time  $t$  is calculated as

$$t(\tau_{m+1}) = t((m+1)\Delta\tau) := \sum_{j=1}^{m+1} \Delta t_j = \Delta\tau \sum_{j=1}^{m+1} L(\tau_j)^2. \quad (4.12)$$

Finally, the numerical solution  $u_j^{(m+1)} \approx u(\xi_j L(\tau_{m+1}), \tau_{m+1})$  can be reconstructed.

Note that as time evolves, the time difference  $T - t(\tau_n)$  will become smaller and smaller, and eventually reach saturation level (with little change), therefore, we treat the stopping time  $t(\tau_{\text{end}}) = t(\tau_M)$  as the blow-up time  $T$ , where  $M$  is the total number of iterations when reaching the stopping condition ( $L < 10^{-24}$ ). Then, we can take

$$T = t(\tau_{\text{end}}) = t(M\Delta\tau) = \Delta\tau \sum_{j=1}^M L(\tau_j)^2. \quad (4.13)$$

Consequently for any  $t_i$ , we calculate  $T - t_i$  as

$$T - t_i = \sum_{j=i+1}^M \Delta t_j = \Delta\tau \sum_{j=i+1}^M L(\tau_j)^2. \quad (4.14)$$

This indicates that instead of recording the cumulative time  $t_i$ , we only need to record the elapsed time between the two recorded data points, i.e.,  $\Delta t_i = t_{i+1} - t_i$ . By doing so, it can avoid the loss of significance when adding a small number onto a larger one.

We construct the artificial boundary condition on the right-hand side from the argument in [41] and [5, Chapter 6.1], since otherwise, the solution to (1.7) has to be solved in the entire space  $\xi > 0$ . For  $\xi \gg 1$ , the nonlinear term and the Laplacian terms is of the higher order compared with the other linear terms, and consequently, can be negligible. Consequently, Eq. (1.7) is reduced to

$$v_\tau + a(\tau) \left( \frac{v}{\sigma} + \xi v_\xi \right) = 0 \quad (4.15)$$

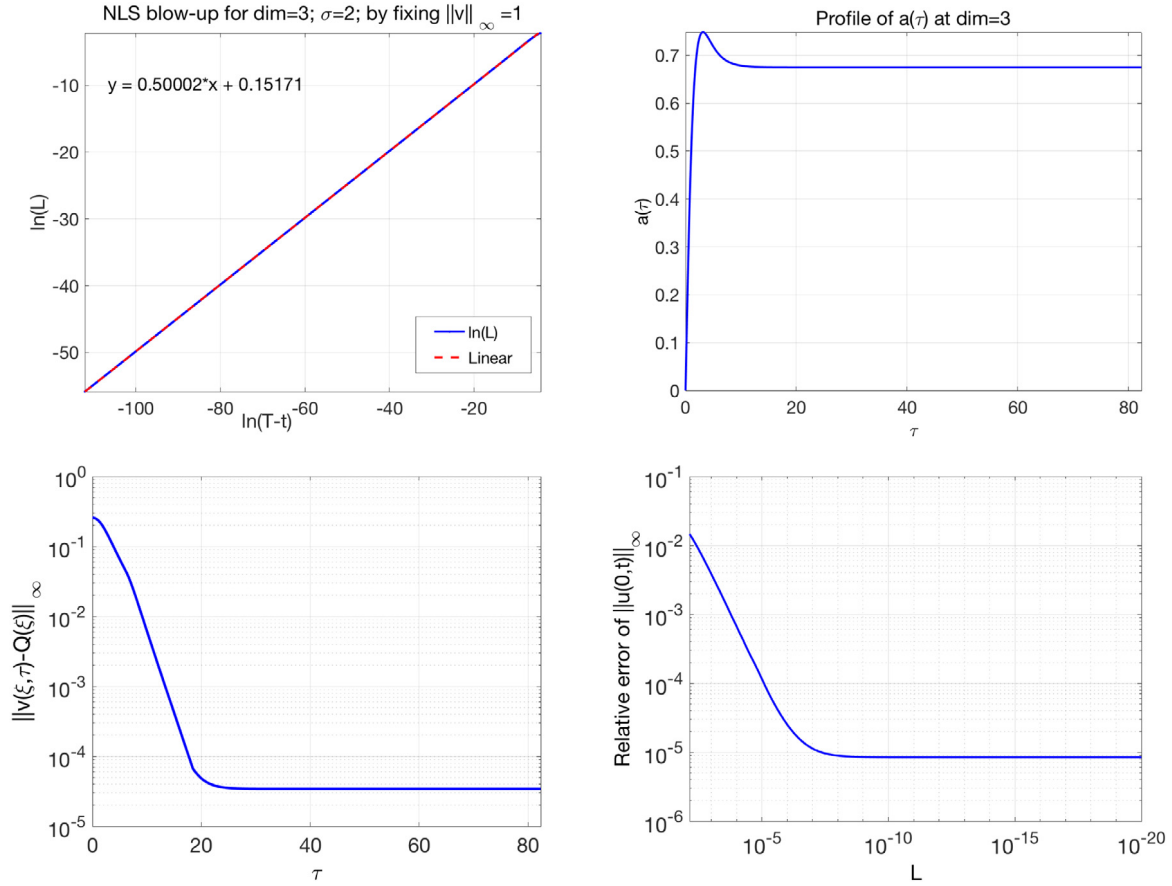


**Fig. 21.** Blow-up data for the 3d quintic case:  $\ln(T-t)$  vs.  $\ln(L)$  (upper left), the quantity  $a(\tau)$  (upper right), the distance between  $Q$  and  $v$  on time  $\tau$  ( $\|v(\tau) - Q\|_{L^\infty}$ ) (lower left), the relative error with respect to the predicted blow-up rate (lower right).

near  $\xi = L_D$ , the right endpoint of the computational domain. Eq. (4.15) can be solved exactly (see [5,41])

$$v(\xi, \tau) = v\left(\xi \frac{L(\tau)}{L(\tau_0)}, \tau_0\right) \left(\frac{L(\tau)}{L(\tau_0)}\right)^{\frac{1}{\sigma}}, \quad (4.16)$$

which suggests that at  $\xi = L_D$ ,

$$v(L_D, \tau_{m+1}) = v\left(L_D \frac{L(\tau_{m+1})}{L(\tau_m)}, \tau_m\right) \left(\frac{L(\tau_{m+1})}{L(\tau_m)}\right)^{\frac{1}{\sigma}}. \quad (4.17)$$

Note that  $a^{(m)} = -\frac{L'(\tau_m)}{L(\tau_m)}$  from (1.8), and  $\frac{L(\tau_m)}{L(\tau_{m-1})}$  can be approximated with the second order accuracy by

$$\frac{L(\tau_m)}{L(\tau_{m-1})} = e^{-\frac{\Delta\tau}{2}(a^{(m-1)} + a^{(m)})} + O(\Delta\tau^3)$$

from (4.10). The value  $L(\tau_{m+1})$  can be approximated by the second order central difference

$$L(\tau_{m+1}) = L(\tau_{m-1}) + 2\Delta\tau L_\tau(\tau_m) + O(\Delta\tau^3). \quad (4.18)$$

Multiplying Eq. (4.18) by  $1/L(\tau_m)$ , we obtain

$$\frac{L(\tau_{m+1})}{L(\tau_m)} = \frac{L(\tau_{m-1})}{L(\tau_m)} - 2\Delta\tau a^{(m)} + O(\Delta\tau^3). \quad (4.19)$$

Therefore, the right-hand side boundary condition is approximated with the second order accuracy

$$v(L_D, \tau_{m+1}) = v\left(L_D(e^{\frac{\Delta\tau}{2}(a^{(m-1)} + a^{(m)})} - 2\Delta\tau a^{(m)}), \tau_m\right) \times \left((e^{\frac{\Delta\tau}{2}(a^{(m-1)} + a^{(m)})} - 2\Delta\tau a^{(m)})\right)^{\frac{1}{\sigma}}. \quad (4.20)$$

Since we are simulating the generic blow-up solutions, the amplitude  $\|u\|_{L^\infty}$  is increasing. Thus, for all  $\tau > 0$ , the term  $\frac{L(\tau_{m+1})}{L(\tau_m)} < 1$ . Taking  $\zeta = L_D \frac{L(\tau_{m+1})}{L(\tau_m)}$ , then  $\zeta$  must be within the computational domain  $[0, L_D]$ , but not necessarily to be one of the grid points. A cubic spline interpolation is adopted to evaluate  $v(\zeta, \tau_m)$  and consequently lead to  $v(L_D, \tau_{m+1})$  from (4.17).

An alternative method for obtaining the artificial boundary condition is to solve Eq. (4.15) numerically, since at the point  $\xi = L_D$ , it reduces to the ODE with respect to  $\tau$ . In [42], the authors solved Eq. (4.15) by using the second order Adam–Bashforth method

$$v(L_D, \tau_{m+1}) = v(L_D, \tau_m) - \frac{1}{2}\Delta\tau \left[ 3a^{(m)} \left( \frac{v(L_D, \tau_m)}{\sigma} + L_D v_\xi(L_D, \tau_m) \right) - a^{(m-1)} \left( \frac{v(L_D, \tau_{m-1})}{\sigma} + L_D v_\xi(L_D, \tau_{m-1}) \right) \right], \quad (4.21)$$

where the terms  $v(L_D, \tau_n) \approx v_N^{(n)}$  and  $v_\xi(L_D, \tau_n)$  is calculated by the six order central difference in space from  $v(L_D, \tau_n)$ , where  $n = m-1$  and  $m$ .

While both numerical boundary conditions (4.20) and (4.21) are of the second order accuracy and lead to the similar results, our numerical experiments suggest that using the method (4.20) allows us to take a larger time step  $\Delta\tau$ .

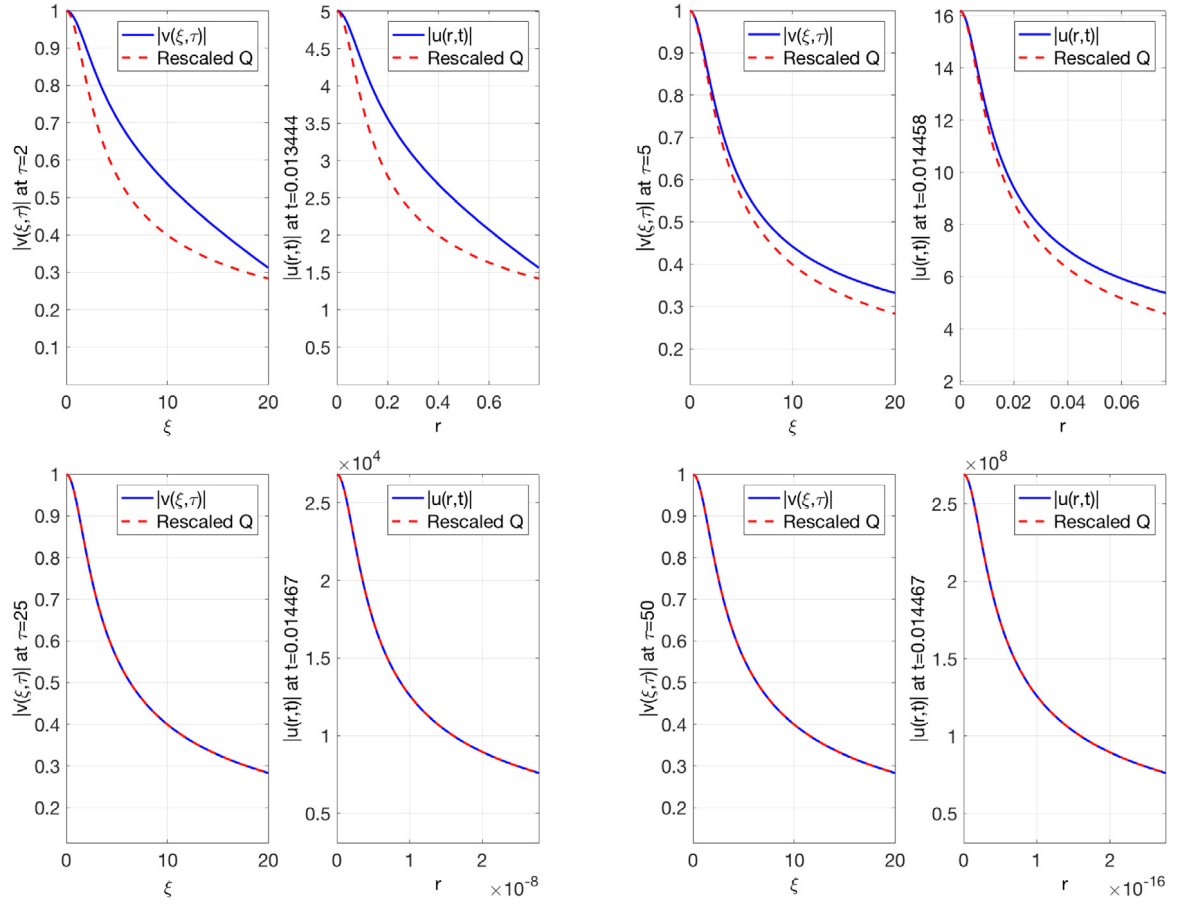


**Fig. 22.** Blow-up profiles for the 4d quintic case at different time  $\tau$  and  $t$ .

#### 4.2. The rescaling of $Q$ and $a$

Recall the solution  $u(r, t)$  to Eq. (1.1) satisfies the self-similar form

$$u(x, t) = \frac{1}{L(t)^{\frac{1}{\sigma}}} Q\left(\frac{x}{L(t)}\right) \exp\left(i\theta + \frac{i}{2a} \log \frac{T}{T-t}\right), \quad (4.22)$$

where  $L(t)$  is predicted to be

$$L_{\text{pred}}(t) \approx (2a(T-t))^{\frac{1}{2}} \quad (4.23)$$

from [24].

Suppose  $Q(\xi)$  is the profile from solving (3.6), and  $\tilde{Q}(\eta)$  is another profile with  $\|\tilde{Q}\|_{L^\infty} = \|v_0(0)\|_{L^\infty}$  (e.g.,  $\|\tilde{Q}\|_{L^\infty} = 1$ ). From (4.22), we have a family of the  $Q$  profiles

$$Q(\xi) = \left(\frac{Q(0)}{\tilde{Q}(0)}\right) \tilde{Q}\left(\xi \left(\frac{Q(0)}{\tilde{Q}(0)}\right)^\sigma\right) \quad (4.24)$$

and consequently, the value  $\tilde{a}$  corresponding to the value  $a$  from (3.6) is

$$\tilde{a} = a \left[ \frac{|v_0(0)|}{Q(0)} \right]^{2\sigma}. \quad (4.25)$$

For simplicity, we still use  $Q$  to represent the family of  $Q$  profiles, adding “up to scaling”.

#### 4.3. Numerical results

In this section, we list examples of initial data we choose and the quantities we track. We take  $h = 0.1$ ,  $k = 10^{-4}/2^{\sigma-2}$ ,  $L_D = 100$  for the dimension  $d = 2, 3$ , and  $L_D = 200$  for the dimension

**Table 1**

Samples of initial conditions  $u_0$  used in our simulations.

$d$	$\sigma$	$u_0$	$E[u_0]$	$u_0$	$E[u_0]$
3	1	$5e^{-r^2}$	$<0$	$\frac{6}{(1+r^2)^4}$	$>0$
4	1	$6e^{-r^2}$	$<0$	$\frac{8}{(1+r^2)^4}$	$>0$
5	1	$6e^{-r^2}$	$<0$	$\frac{8}{(1+r^2)^4}$	$>0$
2	2	$2e^{-r^2}$	$>0$	$\frac{2.5}{(1+r^2)^4}$	$<0$
3	2	$3e^{-r^2}$	$<0$	$\frac{3}{(1+r^2)^4}$	$>0$
4	2	$3e^{-r^2}$	$<0$	$\frac{3}{(1+r^2)^4}$	$>0$
3	3	$2.5e^{-r^2}$	$<0$	$\frac{2.5}{(1+r^2)^4}$	$>0$

$d = 4, 5$ , since larger dimensions may lead the approximation of the artificial boundary condition (4.20) or (4.21) being more reflective, and thus, need larger interval. Other choices of those parameters lead to the similar results (for example, we have tested for  $h = 0.05$  or  $\Delta\tau = 10^{-4}/2^{\sigma-1}$ , see Fig. 13). The initial data is taken to be Gaussian  $u_0 = Ae^{-r^2}$  or rational function with fast enough decay  $u_0 = \frac{A}{(1+r^2)^4}$ . Table 1 lists the examples of initial data together with the energy sign.

In our numerical simulations, the following quantities are of the most interest:

- blow-up profiles  $v(\xi, \tau)$  at different time when approaching blow-up time  $T$ ;
- blow-up rate  $\ln L$  vs.  $\ln(T-t)$ ;
- the value of  $a(\tau)$  with respect to the time  $\tau$ ;

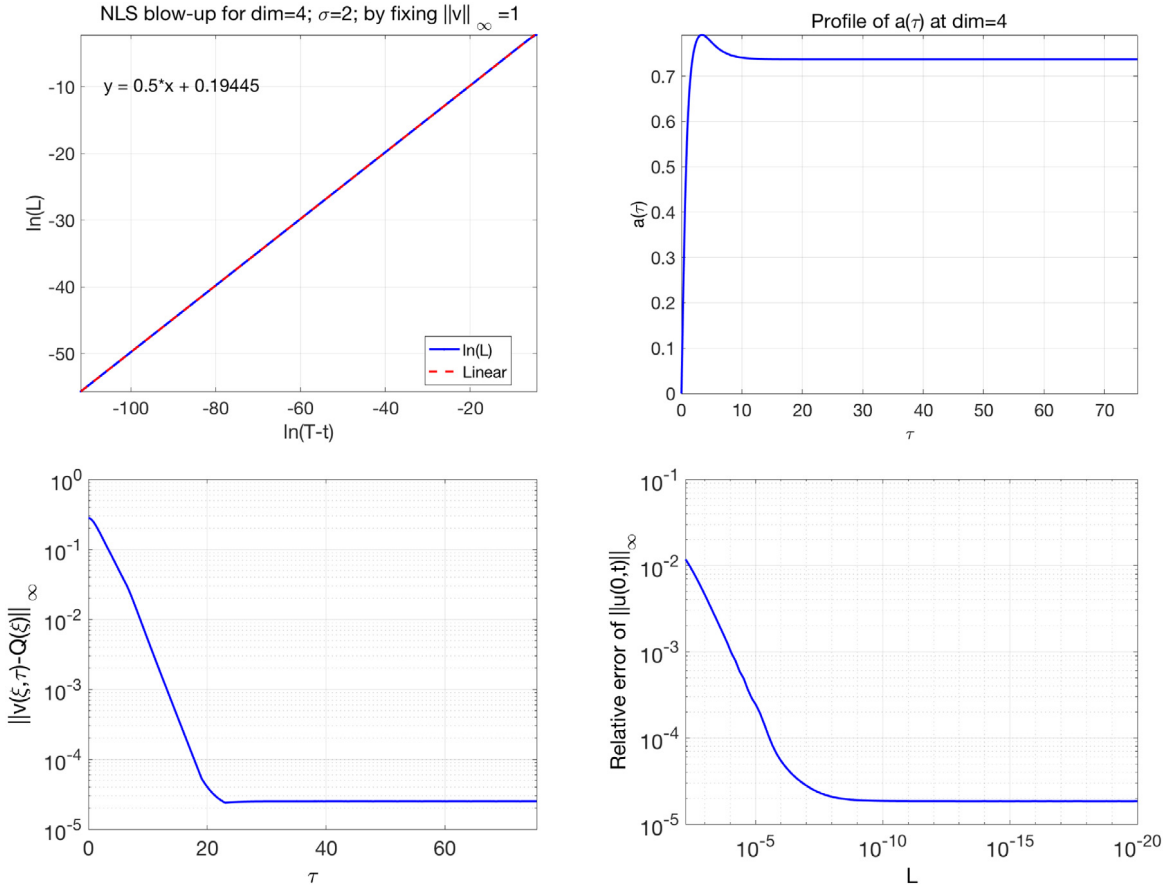


**Fig. 23.** Blow-up data for the 4d quintic case:  $\ln(T-t)$  vs.  $\ln(L)$  (upper left), the quantity  $a(\tau)$  (upper right), the distance between  $Q$  and  $v$  on time  $\tau$  ( $\|v(\tau) - Q\|_{L^\infty}$ ) (lower left), the relative error with respect to the predicted blow-up rate (lower right).

- the dependence of the distance  $\|v(\tau) - Q\|_{L^\infty}$  between  $|Q|$  and  $|v|$  on the rescaled time  $\tau$ ;
- the relative error between blow-up rate and the predicted blow-up rate

$$\mathcal{E}_{rel} = \left| \left( \frac{L(t)}{\sqrt{2\tilde{a}(T-t)}} \right)^{\frac{1}{\sigma}} - 1 \right|,$$

where the value  $\tilde{a}$  is taken to be  $\tilde{a} = a(\tau_{end})$ , i.e., when the stopping criterion reaches

$$L < 10^{-24}. \quad (4.26)$$

Since we track the quantities  $\ln(L)$ ,  $\ln(T-t)$ ,  $a(\tau)$  in the simulations, the relative error  $\mathcal{E}_{rel}$  is calculated as

$$\mathcal{E}_{rel} = \left| \exp \left( \frac{1}{2\sigma} (2\ln(L) - \ln(T-t) - \ln 2 - \ln \tilde{a}) \right) - 1 \right|. \quad (4.27)$$

When each term in (4.27) is moderate (not too large or too small), the accuracy is improved. Note that the value  $\tilde{a}$  can also be calculated from Eq. (4.25), where the values of  $a$  and  $Q(0)$  are obtained from solving Eq. (3.6).

We numerically verify that the  $\tilde{a}$  from these two methods only differs at an order  $10^{-8}$ . This indicates that the profile of  $Q$  obtained in Section 3 is indeed the blow-up profile.

In Fig. 10, the left picture shows the relative error in our simulations ending at  $L \sim 10^{-24}$ , and the right one is up to  $L \sim 10^{-16}$ . The relative error always stays small until the last few points close to our simulation ending time. It suggests that this phenomenon is due to the inaccurate estimation of  $T$ , instead of the solution behavior itself. In the rest of our work, to make it

less confusing, we only show the relative error up to  $L \sim 10^{-20}$ , while we end our simulation at  $L < 10^{-24}$ .

#### 4.4. Consistency verification

We first report the data for the 3d cubic case, which has been considered in [14,27,42], as the purpose of verifying the consistency. Figs. 11 and 12 show the blow-up dynamics for the 3d cubic case. We also track the relative error  $\mathcal{E}_{rel}$  for different  $h$  and  $k$ . As an example, we list the 3d quintic case in Fig. 13, which shows that while the different space step size does not affect the relative error, shrinking the time step will lead to more accurate results.

#### 4.5. Numerical results

We now present our numerical results for different dimensions and nonlinearities.

We first present the *cubic* case in dimensions  $d = 3, 4, 5$ . These cases include  $s_c < 1$ ,  $s_c = 1$  and  $s_c > 1$ , respectively. Fig. 11 shows the blow-up profiles at different times  $\tau$  (or  $t$ ). One can see that the solution converges to the predicted blow-up profile  $Q$ , up to scaling, as  $\tau \rightarrow \infty$  (or  $t \rightarrow T$ ). The two profiles become nearly indistinguishable after  $\tau = 10$ . The top left subplot in Fig. 12 shows that the slope of  $L$  on log scale is still  $\frac{1}{2}$ . The top right subplot in Fig. 12 shows that the parameter  $a(\tau)$  converges to a constant right away (before  $\tau = 10$ ). This indicates that before  $\tau = 10$ , the solution enters the self-similar blow-up regime and explains why the profile  $v(\xi, \tau)$  and the rescaled  $Q$  become indistinguishable right after  $\tau = 10$ . Note that it is

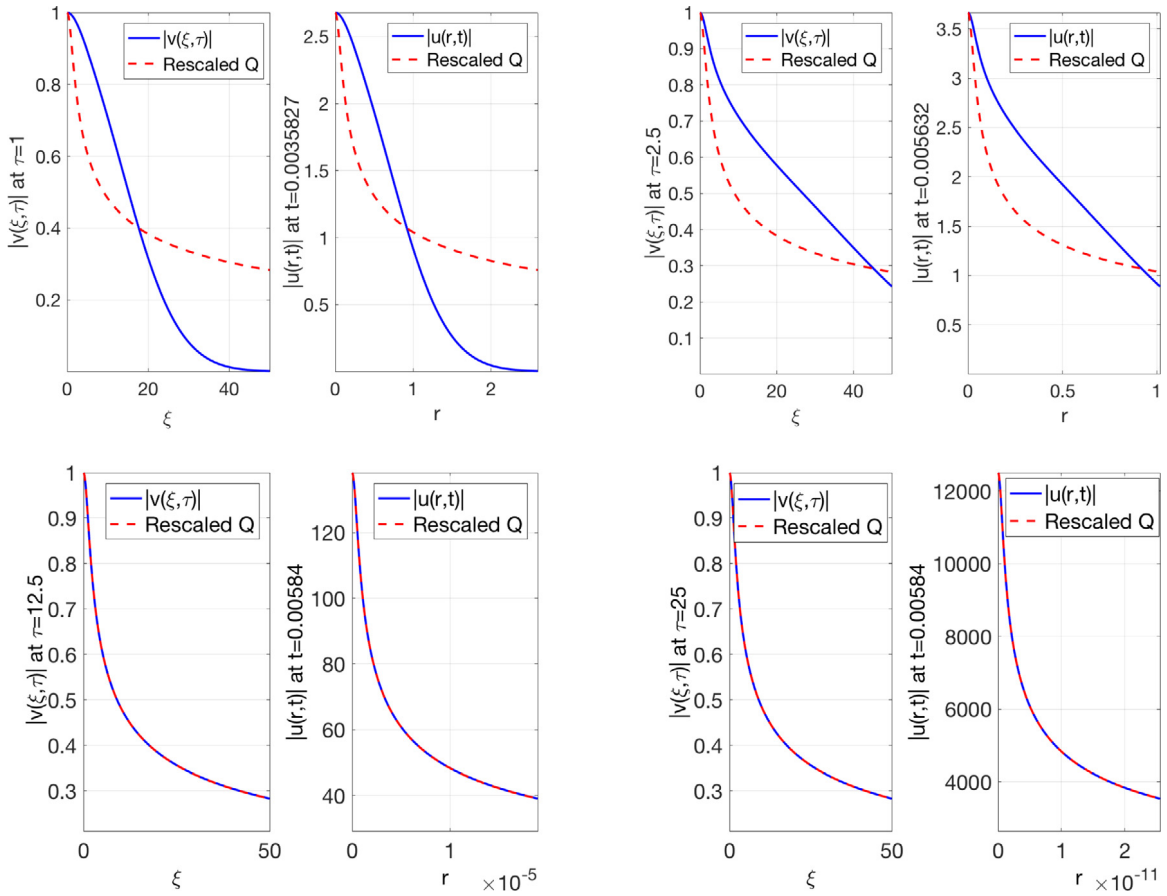


Fig. 24. Blow-up profiles for the 3d septic case at different time  $\tau$  and  $t$ .

not the case for the mass-critical case, where the “log-log” blow-up regime can only be reached at extremely high focusing levels (see e.g. [5,11,12]). The bottom left subplot in Fig. 12 shows the distance between  $|v(\xi, \tau)|$  and the rescaled  $|Q(\xi)|$ . The quantity stabilizes before  $\tau = 10$ , which agrees with the time when the quantity  $a(\tau)$  stabilizes in the top right subplot. The bottom right subplot in Fig. 12 shows the relative error  $\mathcal{E}_{rel}$ . This quantity  $\mathcal{E}_{rel}$  stabilizes at the focusing level  $L \sim 10^{-6}$  with a satisfactory order (around  $10^{-5}$ ). This shows that there is no such “adiabatic” regime occurring before the self-similar regime as the case for the  $L^2$ -critical NLS (see e.g., [7,8,12]).

Figs. 14 and 15 show the results for the 4d cubic case. Both the blow-up profiles and quantities we track are similar to the 3d cubic case. Compared with the 3d cubic case in Figs. 11 and 12, the blow-up profiles become indistinguishable around  $\tau = 50$  (see Fig. 14), and the relative error reaches the stabilized regime around the focusing level  $L \approx 10^{-7}$  (see bottom right subplot in Fig. 15). For the 5d cubic case, besides the similar results to the previous cases (Figs. 16 and 17), from the bottom right subplot in Fig. 17, we see that the relative error reaches a stabilized regime around the focusing level  $L \approx 10^{-8}$ .

We next present the results for the *quintic* case for dimensions  $d = 2, 3, 4$ , see Figs. 18 to 23. We obtain the similar results for these cases as for the cubic cases above. However, by comparing the bottom right subplots in Figs. 19, 21 and 23, we can see that the relative error reaches the stabilized regime at the focusing level  $10^{-6}$ ,  $10^{-7}$  and  $10^{-8}$ , respectively. This shows that for a fixed nonlinearity, the higher dimension leads to the higher focusing level for the solution to reach the self-similar regime. This is also true for the cubic cases (see Figs. 12, 15 and 17).

Finally, we list the 3d *septic* ( $s_c > 1$ ) case in Figs. 24 and 25. While the profiles and results are still similar to the previous

ones, we compare the results for different nonlinearities. Again, the solution reaches the self-similar regime around the focusing level  $L = 10^{-6}$  for the 3d cubic case, around  $L = 10^{-7}$  for the 3d quintic case and around  $L = 10^{-10}$  for the 3d septic case (see the bottom right subplot in Fig. 25). This shows that for a fixed dimension, the higher nonlinearity leads to the higher focusing level for the solution to reach the self-similar regime.

## 5. Conclusion

We generalized the existence and local uniqueness theory of  $Q$  for dimensions  $d \geq 2$  and nonlinearities other than cubic, in the mass-supercritical NLS equations,  $s_c > 0$ . From our numerical simulations, we found that the energy-subcritical, critical and energy-supercritical cases enjoy very similar stable blow-up dynamics. We obtained the self-similar profiles to which stable blow-up solutions converge. Our numerical results show that  $E[Q] = \text{constant}$  if  $s_c = 1$  and  $E[Q] = -\infty$  if  $s_c > 1$ . All these facts show that it maybe challenging to analyze theoretically the stable blow-up dynamics in the mass-supercritical setting. On the other hand, unlike the mass-critical case, certain features of the stable blow-up are easier to exhibit, for example, blow-up solutions converge to the predicted blow-up rate very fast, which can be simply observed numerically, and thus, we do not need to use extended and involved asymptotic analysis on solutions to get information about the rates such as an “adiabatic” regime or the “log-log” regime, which appear in the mass-critical case.

## Acknowledgments

S.R. was partially supported by the NSF, USA CAREER grant DMS-1151618 as well as part of the K.Y.’s graduate research

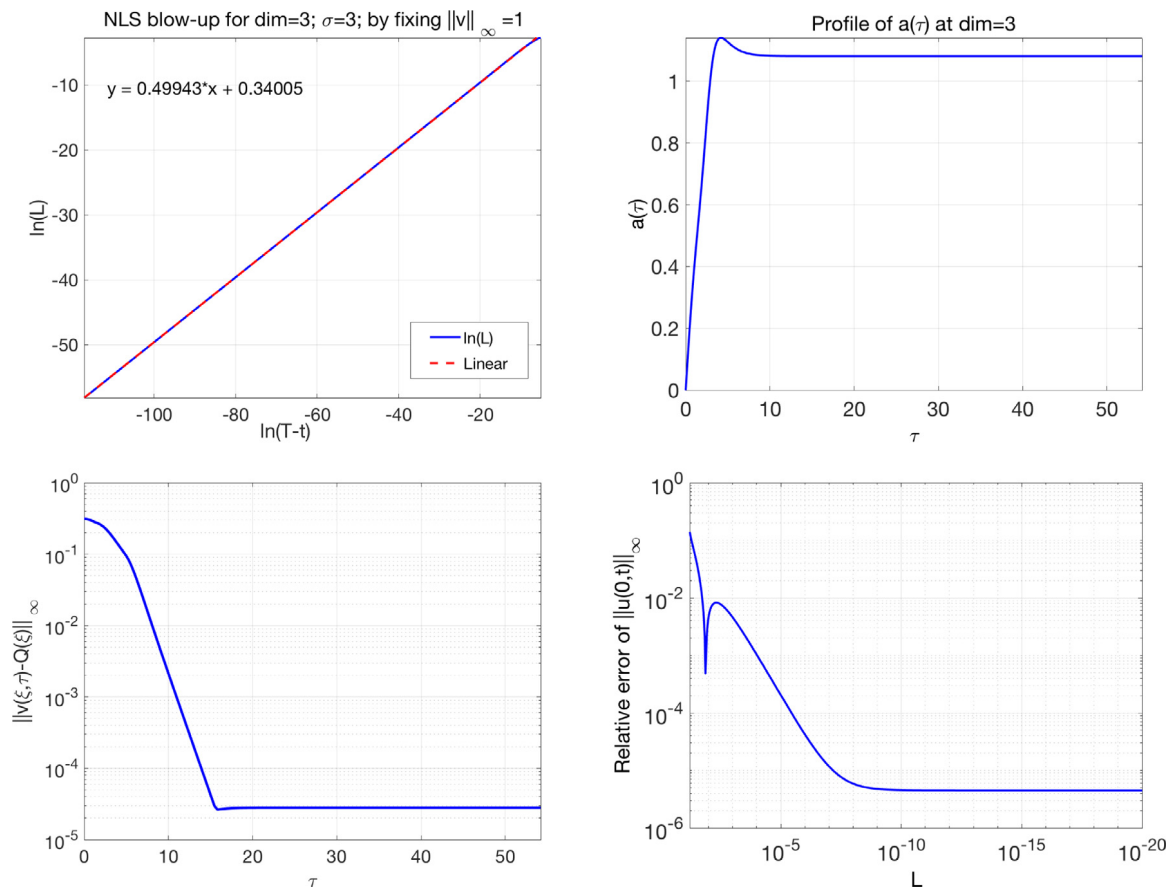


**Fig. 25.** Blow-up data for the 3d septic case:  $\ln(T-t)$  vs.  $\ln(L)$  (upper left), the quantity  $a(\tau)$  (upper right), the distance between  $Q$  and  $v$  on time  $\tau$  ( $\|v(\tau) - Q\|_{L^\infty}$ ) (lower left), the relative error with respect to the predicted blow-up rate (lower right).

fellowship to work on this project came from the above grant. Y.Z. was partially supported by the Columbian College Facilitating Fund, USA (CCFF 2018) and the Simons Foundation, USA through grant no. 357963.

## References

- [1] J. Ginibre, G. Velo, On a class of nonlinear Schrödinger equations. I. The Cauchy problem, general case, *J. Funct. Anal.* 32 (1) (1979) 1–32.
- [2] T. Cazenave, *Semilinear Schrödinger Equations*, in: *Courant Lecture Notes in Mathematics*, vol. 10, New York University, Courant Institute of Mathematical Sciences, American Mathematical Society, New York, Providence, RI, 2003.
- [3] J. Holmer, S. Roudenko, On blow-up solutions to the 3D cubic nonlinear Schrödinger equation, *Appl. Math. Res. Express AMRX* (1) (2007) abm004, 31.
- [4] M.I. Weinstein, The nonlinear Schrödinger equation—singularity formation, stability and dispersion, in: *The Connection Between Infinite-Dimensional and Finite-Dimensional Dynamical Systems* (Boulder, CO, 1987), in: *Contemp. Math.*, vol. 99, Amer. Math. Soc, Providence, RI, 1989, pp. 213–232.
- [5] C. Sulem, P.-L. Sulem, *The Nonlinear Schrödinger Equation*, in: *Applied Mathematical Sciences*, vol. 139, Springer-Verlag, New York, 1999, Self-focusing and wave collapse.
- [6] G. Perelman, On the blow up phenomenon for the critical nonlinear Schrödinger equation in 1D, in: *Nonlinear dynamics and renormalization group* (Montreal, QC, 1999), in: *CRM Proc. Lecture Notes*, vol. 27, Amer. Math. Soc, Providence, RI, 2001, pp. 147–164.
- [7] G. Fibich, G. Papanicolaou, A modulation method for self-focusing in the perturbed critical nonlinear Schrödinger equation, *Phys. Lett. A* 239 (3) (1998) 167–173.
- [8] G. Fibich, G. Papanicolaou, Self-focusing in the perturbed and unperturbed nonlinear Schrödinger equation in critical dimension, *SIAM J. Appl. Math.* 60 (1) (2000) 183–240.
- [9] G. Fibich, N. Gavish, X.-P. Wang, New singular solutions of the nonlinear Schrödinger equation, *Physica D* 211 (3–4) (2005) 193–220.
- [10] G. Fibich, N. Gavish, X.-P. Wang, Singular ring solutions of critical and supercritical nonlinear Schrödinger equations, *Physica D* 231 (1) (2007) 55–86.
- [11] G. Fibich, *The Nonlinear Schrödinger Equation*, in: *Applied Mathematical Sciences*, vol. 192, Springer, Cham, 2015, Singular solutions and optical collapse.
- [12] K. Yang, S. Roudenko, Y. Zhao, Blow-up dynamics and spectral property in the  $L^2$ -critical nonlinear Schrödinger equation in high dimensions, *Nonlinearity* 31 (9) (2018) 4354–4392.
- [13] D. McLaughlin, G. Papanicolaou, C. Sulem, P. Sulem, Focusing singularity of the cubic Schrödinger equation, *Phys. Rev. A* 34 (1986) 1200–1210.
- [14] M.J. Landman, G.C. Papanicolaou, C. Sulem, P.-L. Sulem, Rate of blowup for solutions of the nonlinear Schrödinger equation at critical dimension, *Phys. Rev. A* (3) 38 (8) (1988) 3837–3843.
- [15] G.D. Akrivis, V.A. Dougalis, O.A. Karakashian, W.R. McKinney, Numerical approximation of blow-up of radially symmetric solutions of the nonlinear Schrödinger equation, *SIAM J. Sci. Comput.* 25 (1) (2003) 186–212.
- [16] G. Fibich, F. Merle, P. Raphaël, Proof of a spectral property related to the singularity formation for the  $L^2$  critical nonlinear Schrödinger equation, *Physica D* 220 (1) (2006) 1–13.
- [17] F. Merle, P. Raphaël, Profiles and quantization of the blow up mass for critical nonlinear Schrödinger equation, *Comm. Math. Phys.* 253 (3) (2005) 675–704.
- [18] G. Perelman, On the formation of singularities in solutions of the critical nonlinear Schrödinger equation, *Ann. Henri Poincaré* 2 (4) (2001) 605–673.
- [19] F. Merle, Determination of blow-up solutions with minimal mass for nonlinear Schrödinger equations with critical power, *Duke Math. J.* 69 (2) (1993) 427–454.
- [20] P. Raphaël, Stability of the log-log bound for blow up solutions to the critical non linear Schrödinger equation, *Math. Ann.* 331 (3) (2005) 577–609.
- [21] F. Merle, P. Raphaël, Sharp upper bound on the blow-up rate for the critical nonlinear Schrödinger equation, *Geom. Funct. Anal.* 13 (3) (2003) 591–642.
- [22] B. LeMesurier, G. Papanicolaou, C. Sulem, P.-L. Sulem, The focusing singularity of the nonlinear Schrödinger equation, in: *Directions in partial differential equations* (Madison, WI, 1985), in: *Publ. Math. Res. Center Univ. Wisconsin*, Vol. 54, Academic Press, Boston, MA, 1987, pp. 159–201.

- [23] V.E. Zakharov, Collapse and self-focusing of langmuir waves, in: A.A. Galeev, R.N. Sudan (Eds.), *Basic Plasma Physics: Selected Chapters*, in: *Handbook of Plasma Physics*, vol. 1, 1984, p. 81.
- [24] B.J. LeMesurier, G.C. Papanicolaou, C. Sulem, P.-L. Sulem, Local structure of the self-focusing singularity of the nonlinear Schrödinger equation, *Physica D* 32 (2) (1988) 210–226.
- [25] V. Zakharov, E. Kuznetsov, Quasi-classical theory of three-dimensional wave collapse, *Zh. Eksp. Teor. Fiz.* 91 (1986) 1310–1324.
- [26] X.P. Wang, *On Singular Solutions of the Nonlinear Schroedinger and Zakharov Equations*, (Thesis (Ph.D.)–New York University), ProQuest LLC, Ann Arbor, MI, 1990.
- [27] C.J. Budd, S. Chen, R.D. Russell, New self-similar solutions of the nonlinear Schrödinger equation with moving mesh computations, *J. Comput. Phys.* 152 (2) (1999) 756–789.
- [28] B.J. LeMesurier, G. Papanicolaou, C. Sulem, P.-L. Sulem, Focusing and multi-focusing solutions of the nonlinear Schrödinger equation, *Physica D* 31 (1) (1988) 78–102.
- [29] N. Kopell, M. Landman, Spatial structure of the focusing singularity of the nonlinear Schrödinger equation: a geometrical analysis, *SIAM J. Appl. Math.* 55 (5) (1995) 1297–1323.
- [30] F. Merle, P. Raphaël, J. Szeftel, Stable self-similar blow-up dynamics for slightly  $P^2$  super-critical nls equations, *Geom. Funct. Anal.* 20 (4) (2010) 1028–1071.
- [31] V. Rottschäfer, T.J. Kaper, Blowup in the nonlinear Schrödinger equation near critical dimension, *J. Math. Anal. Appl.* 268 (2) (2002) 517–549.
- [32] C.J. Budd, Asymptotics of multibump blow-up self-similar solutions of the nonlinear Schrödinger equation, *SIAM J. Appl. Math.* 62 (3) (2002) 801–830.
- [33] C. Budd, O. Koch, E. Weinmüller, Computation of self-similar solution profiles for the nonlinear Schrödinger equation, *Computing* 77 (4) (2006) 335–346.
- [34] C.J. Budd, W. Huang, R.D. Russell, Adaptivity with moving grids, *Acta Numer.* 18 (2009) 111–241.
- [35] V. Rottschäfer, T.J. Kaper, Geometric theory for multi-bump, self-similar, blowup solutions of the cubic nonlinear Schrödinger equation, *Nonlinearity* 16 (3) (2003) 929–961.
- [36] T.A. Burton, *Volterra Integral and Differential Equations*, second ed., in: *Mathematics in Science and Engineering*, vol. 202, Elsevier B. V, Amsterdam, 2005.
- [37] L.N. Trefethen, *Spectral Methods in MATLAB*, in: *Software, Environments, and Tools*, vol. 10, Society for Industrial and Applied Mathematics (SIAM), Philadelphia, PA, 2000.
- [38] J. Shen, T. Tang, L.-L. Wang, *Spectral Methods*, in: *Springer Series in Computational Mathematics*, vol. 41, Springer, Heidelberg, 2011, Algorithms, analysis and applications.
- [39] W. Ren, X.-P. Wang, An iterative grid redistribution method for singular problems in multiple dimensions, *J. Comput. Phys.* 159 (2) (2000) 246–273.
- [40] A. Ditzkowski, N. Gavish, A grid redistribution method for singular problems, *J. Comput. Phys.* 228 (7) (2009) 2354–2365.
- [41] S.V.N.E. Kosmatov, V. Zakharov, Computer simulation of wave collapses in the nonlinear Schrödinger equation, *Physica D* 52 (1991) 16–35.
- [42] M.J. Landman, G.C. Papanicolaou, C. Sulem, P.-L. Sulem, X.P. Wang, Stability of isotropic singularities for the nonlinear schrödinger equation, *Physica D* 47 (3) (1991) 393–415.